An Investigation on the Morphological Evolution of Bright-Rimmed Clouds(BRCs)

Jingqi Miao[1], Glenn, J. White[2,3], M. A. Thompson[4], Richard P. Nelson[5]

ABSTRACT

A new Radiative Driven Implosion (RDI) model based on Smoothed Particle Hydrodynamics (SPH) technique is developed and applied to investigate the morphological evolutions of molecular clouds under the effect of ionising radiation. This model self-consistently includes the self-gravity of the cloud in the hydrodynamical evolution, the UV radiation component in the radiation transferring equations, the relevant heating and cooling mechanisms in the energy evolution and a comprehensive chemical network. The simulation results reveal that under the effect of ionising radiation, a molecular cloud may evolve through different evolutionary sequences. Dependent on its initial gravitational state, the evolution of a molecular cloud does not necessarily follow a complete morphological evolution sequence from type A→B→C, as described by previous RDI models. When confronted with observations, the simulation results provide satisfactory physical explanations for a series of puzzles derived from Bright-Rimmed Clouds(BRCs) observations. The consistency of the modelling results with observations shows that the self-gravity of a molecular cloud should not be neglected in any investigation on the dynamical evolution of molecular clouds when they are exposed to ionising radiation.

Subject headings: star: formation – ISM: evolution – ISM: HII regions – ISM: kinematics and dynamics – radiative transfer.

[1]Centre for Astrophysics & Planetary Science, School of Physical Sciences, University of Kent, Canterbury, Kent CT2 7NR, UK, J.Miao@kent.ac.uk

[2]Centre for Earth, Planetary, Space & Astronomical Research, The Open University, Walton Hall, Milton Keynes, MK7 6AA

[3]Space Physics Division, Space Science & Technology Division, CCLRC Rutherford Appleton Laboratory, Chilton, Didcot, Oxfordshire, OX11 0QX, UK

[4]School of Physics Astronomy & Maths, University of Hertfordshire, College Lane, Hatfield, AL10 9AB, UK

[5]School of Mathematical Sciences, Queen Mary College, University of London, Mile End Road, London E1 4NS, UK

1. Introduction

Bright-rimmed clouds (BRCs) found in and around HII regions are sites of ongoing star formation due to compression by ionisation/shock fronts, and provide an excellent laboratory to study the influence of UV radiation from nearby massive stars on the evolutionary process of molecular clouds. Numerous molecular line, millimetre/sub-millimetre continuum and mid-IR surveys have revealed very detailed structures and physical properties of BRCs in various astrophysical environments (Sugitani et al 1991; Sugitani & Ogura 1994; Thompson et al 2004a,b; Thompson & White 2004; Urquhart et al 2006).

One of the most intriguing characteristics of the observed BRCs is the diversity of their morphologies. The observed BRCs appear in different morphologies even when they are in similar stellar environments. Sugitani et al (1991, 1994) classified 89 BRCs from a whole sky survey into three types depending on the curvature of the rim of BRCs. The three types are categorised with type A cloud with a rim displaying moderate curvature, type B cloud with a rim of a high degree of curvature which sometimes is also described as an elephant trunk morphology, and finally type C cloud with a tightly curved rim and a tail, which is also called cometary globule.

Lefloch & Lazareff (1994) presented a 2-dimensional numerical simulation of the effect of UV radiation on the dynamical evolution of a molecular cloud based on the Radiation Driven Implosion (RDI) model. Although their hydrodynamical modelling successfully created a complete sequence of the morphological evolution of a molecular cloud from type A to B and then to C, it seems difficult to provide physical explanations for the following questions derived from BRC observations:

1) Why are there so many more type A BRCs? The first whole sky survey by Sugitani et al (1991,1994) revealed that 61% of the observed 89 BRCs have type A morphology. If all of the clouds followed the same evolutionary sequence revealed by Lofloch's modelling, from type A to type C morphology, there should be a balanced number of BRCs with different morphologies to be observed.

2) Why do some of observed BRCs evolve to a quasi-stable type A rimmed morphology and show signs of star formation at the heads of their structures? If all of the clouds should evolve to type C morphology and finally were completely photoevaporated as described by Lelfloch's modelling, no star formation should be triggered in type A BRCs. The recent radio continuum and molecular line observations on BRCs in the catalogue of SFO (Sugitani et al 1991; Sugitani & Ogura 1994) presented by Urquhart et al (2006) and many other observations in molecular lines and submilimeter lines (Lee et al 2005; Karr & Martin 2003; Thompson et al 2004b) provided strong evidences of ongoing star formations in the condensed head of type

A rimmed clouds where a pressure equilibrium at the boundary between the clouds and its environment has been reached. Therefore it seems that for some of the molecular clouds, further evolution to type B or C rimmed morphologies is not necessary, i.e., not every BRC's morphological evolution follows the sequence from type A to B then to C rimmed morphology, it may terminate their morphological evolution at any one of the three morphologies.

3) What causes the spatial morphological distribution of BRCs in some of molecular cloud clusters? The remnant molecular clouds in the Ori OB 1 associations (Ogura & Sugitani 1998) presented a spatial sequence from type A→B→C rimmed BRCs with their distance from the ionising star. It was once suggested that some molecular clouds which were farther away may directly evolve to type C rimmed morphology (Ogura & Sugitani 1998), but there is no physical foundation for this speculation.

For the molecular clumps very close to an ionising star, the ionised gas cannot expand freely from the surface of the clump, because their expansion is constrained by a material flow accompanying with the ionisation radiation flux. Lefloch's simulation showed that a zero radial velocity boundary condition, (the extreme case of flow effect) favours the type A BRC formation (Lefloch & Lazareff 1994). This result may partly explain the predominance of type A BRCs at the border of the HII regions. However question remains for the type A BRC structures found at the outer location of the HII regions or type B/C BRCs found at the border of HII regions (Sugitani et al 1991; Sugitani & Ogura 1994) and there are must be some other physical mechanisms which play dominant roles in the morphological evolution of molecular clouds.

Therefore searching for satisfactory solutions to the above puzzles requires a more comprehensive model which should include as many physical processes as possible so that reliable physical explanations on what observations revealed can be derived, hence to greatly improve our understanding on how the intensive UV radiation from nearby stars affects the dynamical evolution of the surrounding molecular clouds.

The fact that IRAS sources and bipolar outflows in cloud globules are very often found at the edges of BRCs strongly suggests that the self-gravity of a molecular cloud can play an active role even in the early stages of evolution in molecular clouds (Lefloch & Lazareff 1994). Nevertheless the self-gravity of a molecular cloud was neglected in Lefloch's model, because the initiative of the model was to investigate photo-evaporation effect of molecular clouds, for which self-gravity does not play a dominant role. However, as pointed out by Lefloch & Lazareff (1994) at the end of the discussions of their modelling results, inclusion of the self-gravitation of a molecular cloud is necessary in order to build a appropriate model for investigation on the dynamical evolution of globule clouds under the effect of UV radiation.

Recently, Kessel-Deynet & Burkert (2000, 2003) have developed the first 3-D SPH RDI model for investigation of the effect of UV radiation on the dynamical evolution of molecular clouds. Their model includes both self-gravity and the hydrogen ionisation of the molecular cloud in the dynamical evolution equations and revealed further features of molecular cloud evolution under the effect of ionising radiation. However a self-consistent treatment for the energy evolution was not included which sets a barrier for a rigorous study on the evolution of the physical properties of a cloud, so that a direct confrontation with observations is difficult.

Therefore it is our intention to build a comprehensive RDI model in order to obtain a consistent description about the effect of the UV radiation on the dynamical evolution of a molecular cloud and to reveal the physical origin for the observed characteristics of BRCs' morphology formation.

In the following sections we first give an outline for our 3-D RDI model, then briefly present an analytical solution which uses some observable physical properties of a condensed globule and the UV radiation flux to define a maximum mass a stable condensed globule could have to against the gravitational collapse. Next the dynamical evolution of the cloud will be detailed and the corresponding kinematics will be analysed based on numerical simulation results. Finally we will apply the derived knowledge to confront with BRCs' observations and the conclusions are drawn at the end of the paper.

2. The model

In this section, we present a brief description of the basic equations and various physical processes included in our model. The hydrodynamical equations are solved with Smoothed Particle Hydrodynamical(SPH) technique. For the detailed description of the SPH theory and the corresponding technique, readers are directed to Nelson & Langer (1999).

2.1. The basic dynamical equations

The continuity, momentum, and energy equations for a compressible fluid can be written as:

$$\frac{d\rho}{dt} + \rho\nabla\cdot\mathbf{v} = \mathbf{0} \tag{1}$$

$$\frac{d\mathbf{v}}{dt} = -\frac{1}{\rho}\nabla P - \nabla\Phi + \mathbf{S_{visc}} \tag{2}$$

$$\frac{d\mathcal{U}}{dt} + \frac{P}{\rho}\nabla \cdot \mathbf{v} = \frac{\gamma - \mathbf{\Lambda}}{\rho} \tag{3}$$

and the chemical rate equations take the general form:

$$\frac{dX_i}{dt} = nK_i \tag{4}$$

where $d/dt = \partial/dt + \mathbf{v} \cdot \nabla$ denotes the convective derivative, ρ is the density; $\mathbf{v}$ is the velocity; P is the pressure; $\mathbf{S_{visc}}$ represents the viscous forces; $\mathcal{U}$ is the internal energy per unit mass; and Φ is the gravitational potential. γ and Λ represent the non adiabatic heating and cooling functions respectively, which we will deal with later; The fractional abundance of main chemical species X_i in Equation (4) are for CO, CI, CII, HCO^+, OI, He^+, H_3^+, OH_x, CH_x, M^+ and electrons; K_i is the associated chemical reaction rate and n is the total number density.

2.2. Ionising radiation transfer

The molecular cloud in our model is under the effects of both UV and FUV radiation fields. The UV radiation is from a nearby star and interacts with the molecular cloud through the top layer of the surface facing the star (front surface). The FUV radiation onto the front surface is from the nearby star and that onto the rear surface is from the background star light (Nelson & Langer 1999). Then the FUV radiation field around a molecular cloud can be approximated as a spherical radiation field (Gorti & Hollenbach 2002). The the effect of the FUV field on the molecular cloud is mainly through the photoelectric emission of electrons from grains and is treated in the same way as that in Nelson & Langer (1999). In the following part of this subsection we only need discuss how to deal with the ionising radiation (UV) field from the nearby star.

Although Helium ionisation was included in the chemical network, we could safely neglect it when dealing with the ionisation radiation transfer, ionisation heating and cooling for simplicity, because of the much lower abundance of the Helium compared to hydrogen atoms (Dyson & Williams 1997). The implementation of ionising radiation from nearby stars into the above SPH code is based on solving the following ionisation rate and radiative transfer equations,

$$\frac{dn_e}{dt} = \mathcal{I} - \mathcal{R} \tag{5}$$

$$\frac{dJ}{dz} = -\sigma n(1-x)J \tag{6}$$

where $\mathcal{I} = \sigma n(1-x)J$ is the ionisation rate with σ being the effective ionisation cross section; $\mathcal{R} = n_e^2\alpha_B = x^2n^2\alpha_B$ is the recombination rate with α_B being the effective recombination

coefficient under the assumption of the 'on the spot' approximation (Dyson & Williams 1997). In its original definition, the recombination coefficient

$$\alpha = \sum_i \alpha_i$$

includes all of the individual recombination coefficients α_i to the hydrogen atomic energy level i. In the 'on the spot' assumption, recombinations into the ground level ($i = 1$) do not lead to any net effect on the change in ionisation rate, since the photons released from this recombination process are able to re-ionise other hydrogen atoms on the spot. Therefore α_1 can be neglected and the resulting net recombination coefficient can be written as

$$\alpha_B = \sum_{i=2}^{\infty} \alpha_i$$

For a planner infall of ionising photons from a distant source on the boarder with a flux J_0 as the Lyman continuum photons per unit time and square area, the solution of Eq.(6) is

$$J(z) = J_0\, exp[-\tau(z)]$$

where $\tau(z)$ is the optical depth for ionising photons along the line of sight parallel to the infall direction of the photons, and z is the distance from the border of the integration volume along the line of sight. Neglecting the absorption effect of dust on ionising radiation, $\tau(z)$ can be expressed as (Kessel-Deynet & Burkert 2000)

$$\tau(z) = \int_R^z n_H(z')\ \bar{\sigma}\ dz' \tag{7}$$

with $n_H = n(1 - x)$ and $\bar{\sigma}$ being the mean of σ_v over frequency, weighted by the spectrum of the source (Kessel-Deynet & Burkert 2000).

Eq.(6) can be written in terms of the ionisation ratio x, i.e.,

$$\frac{dx}{dt} \ = \ \frac{1}{n}\frac{dn_e}{dt} = \frac{\mathcal{I}}{n} - x^2 n\alpha_B \tag{8}$$

Solving Eq.(8) for the ionising ratio x includes three steps: i.e., calculate the optical path $\tau(z)$; calculate the ionising rate I and then finally integrate Eq.(8) for x. We employ the method introduced by Kessel-Deynet & Burkert (2000) in the above three-step work. We just give a very short description about it here. The interested reader can find more detailed description in Kessel-Deynet & Burkert (2000).

For any a simulated particle i with its number density n and its nearest neighbour list being given by the dynamical simulation at each time step, calculating $\tau(z)$ is carried

through a) finding the evaluation points on the path toward source by smallest angel criteria and then b)summing up all the optical path elements on the path

$$\tau(z_i) = \Sigma_{k=0}^{m}\ \bar{\sigma}\ n_{H,k}\ \Delta z_k$$

where m is the total number of the evaluation points from the boundary of the volume to the position located one effective radius ($a_i = 0.85(M_i/\rho_i)^{1/3}$) before the point z_i which is derived from a); $n_{H,k}$ is the number density of the hydrogen atoms at the evaluation point k, M_i and ρ_i are the mass and mass density of the particle i respectively.

The ionisation rate for the particle i is then calculated by

$$I_i = \frac{J_0}{2a_i n_i} exp[-\tau(z_i)]\ [1 - exp(-2a_i\, n_{H,i})]$$

Finally, the first-order discretisation of Eq. (8) over a time interval Δt for particle i is given by

$$x_i^{j+1} = x_i^j + \Delta t\ [\frac{\mathcal{I}_i^{j+1}}{n_i^{j+1}} - n_i^{j+1}\,(x_i^2)^{j+1}\alpha_B] \tag{9}$$

where the indexes j and $j+1$ denote the values at the beginning and the end of the actual time-step δt respectively. All of the values on the right-hand side are known from advancing the particles by the SPH formalism, except $\mathcal{I}_i^{j+1}$, which can be approximated by

$$\mathcal{I}_i^{j+1} = \mathcal{I}_i^j \frac{1 - exp[-\bar{\sigma} n_{H,i}^{j+1}\, a_i^{j+1}]}{1 - exp[-\bar{\sigma} a_i^{j+1} n_{H,i}^j]} \tag{10}$$

2.3. The heating function γ

The heating function in the thermal evolution is mainly provided by a) the photoelectric emission of electrons from grains γ_{pe} caused by the incident FUV component ($6.5 < h\nu < 13.6$ eV) of background star light, which can be treated as isotropic and has been discussed by Nelson & Langer (1999). so we don't repeat them here; b) the hydrogen ionisation heating γ_{ion} produced by the illumination of UV component ($h\nu > 13.6$eV) from a nearby massive star, which is highly directional and whose strength is dependent on the distance of the cloud from the star. Its formula can be derived through the following considerations.

When an atom with ionisation energy E_1 is ionised following the absorption of one photon of frequency ν and energy $E = h\nu$, it releases one electron which carries the excess kinetic energy $E_\nu - E_1$ which will be transfered to the gas through collisions with other gas particles. The resulting heating rate is described by the following equation.

$$\gamma_{ion} = n(1-x)\sigma JkT_* \tag{11}$$

where k is the Boltzmann constant and T_* is expressed as (Cantó et al 1998)

$$T_* = T_{eff}\frac{x_0^2 + 4x_0 + 6}{x_0^2 + 2x_0 + 2} \tag{12}$$

where T_{eff} is the stellar temperature, and $x_0 = (h\nu_0)/(kT_{eff})$ with ν_0 being the frequency of the Lyman limit.

Heating of the gas is also affected by cosmic ray heating, H_2 formation heating and gas-dust thermal exchange, for which the same formulae as that in (Nelson & Langer 1999) are used in our model.

2.4. The cooling function Λ

The cooling function Λ is affected by recombination of the electrons with ions, the collisional excitation of OII lines and by CO, CI, CII and OI line emission.

When a free electron in the plasma is captured by a proton, a photon is emitted and an amount of energy $E_1 + m_e v_e^2/2$ is removed from the internal energy of the gas. The cooling rate due to this process is (Hummer & Seaton 1963)

$$\Lambda_{rec} = \beta_B\, n^2 x^2 kT \tag{13}$$

where $\beta_B = \alpha_B \times (1 + 0.158t_e)$.

Another important cooling resource comes from the collisional excitation of low-lying energy levels of OII ions in spite of their low abundance, since OII has energy levels with excitation potentials of the order of kT. We use the following simplified formula derived by Raga et al (2002) to calculate the cooling rate due to the collisional excitation of OII,

$$\Lambda_{colli} = \Lambda_{colli\,(1)} + \Lambda_{colli\,(2)} \tag{14}$$

with

$$log_{10}[\frac{\Lambda_{colli\,(1)}}{n_e n_{OII}}] = 7.9t_1 - 26.8 \tag{15}$$

$$log_{10}[\frac{\Lambda_{colli\,(2)}}{n_e n_{OII}}] = 1.9\frac{t_2}{|t_2|^{0.5}} - 20.5 \tag{16}$$

with $t_1 = 1 - 2000$ K$/T$ and $t_2 = 1 - 5 \times 10^4$ K$/T$ and $n_{OII} = x n_{OI}$. The above formula is valid under the limit of low electron density $n_e < 10^4$ cm^{-3}, which is true for the BRCs' structure.

The cooling affects Λ_{line} by CO, CI, CII and OI line emission are same as those in the Nelson & Langer (1999).

2.5. Boundary conditions and initial velocity field

The molecule cloud is assumed to have a spherical symmetry and its mass is uniformly distributed through a sphere of radius R. It is embedded in surrounding hot medium with a constant density (HII region) (Kessel-Deynet & Burkert 2003). The external pressure by the surrounding hot medium provides an inwardly directed pressure force whose characteristic magnitude is similar to that expected from a HII region. The value of the assumed boundary pressure P_{ext} we adopted here is equivalent to an ionised gas with $n_e = 100\mathrm{cm}^{-3}$ and $T = 10^4\mathrm{K}$(Lefloch et al 2002), which resembles to Lefloch's zero radial velocity boundary condition.

An outflow condition is imposed at a fixed radius equal to several times of the original radius of the cloud. Material that expand beyond this radius is simply removed from the calculation. By this time, these particles represent very low density material and so provide little UV extinction or other influence in the simulations.

The initial turbulent velocity field was set up in the usual manner, as described by Mac Low et al (1998), with perturbations set up with a flat power spectrum $P(k)$, and with a minimum wavenumber k_{min} corresponding to a wavelength equal to the cloud diameter. Eight wave numbers were used to set up the velocity perturbations with the maximum, $k_{max} = 8\,k_{min}$. The velocity perturbations were drawn from a Gaussian random field determined by its power spectrum in Fourier space. For each three dimensional wavenumber k, we randomly select an amplitude from a Gaussian distribution centred on zero, and of height $P(k)$, and selected a random phase uniformly distributed between 0 and 2π. The field is then transformed back into real space to get the real velocity for each particle, and then multiplied by the amplitude needed to obtain the required total kinetic energy for the cloud. This procedure is repeated for each velocity component independently to get the full three dimensional velocity field. The amplitude of the turbulent motion was normalised such that the total kinetic energy of the clouds equals their initial gravitational potential energy.

The initial geometry of the cloud and radiation field configurations are shown in Figure 1. Since the distance of the cloud to the nearby illuminating star is assumed to be large compared to the radius of the cloud, the UV radiations from the star can then be treated as a plane-parallel radiation onto the front surface of the cloud (Lefloch & Lazareff 1994; Kessel-Deynet & Burkert 2000; Willams et al. 2001) while the FUV radiation is isotropic to the cloud (Gorti & Hollenbach 2002; Nelson & Langer 1999)

The radiation flux distribution at the boundary is

$$J(r=R,\theta)=\begin{cases} J_0(\text{Lyman})+J_0(\text{FUV}) & 0^o\leq\theta\leq 90^o) \\ J_0(\text{FUV}) & 90^o\leq\theta\leq 180^o) \end{cases}$$

where J_0(Lyman) is the value of the Lyman continuum flux at the surface of the cloud for which we take the typical value of 2×10^{11} cm^{-2} s^{-1} (Miao et al 2006; Willams et al. 2001); J_0(FUV) is the value of the interstellar radiation at the surface of the cloud which has the value of $100\times G_0$, where G_0 is the mean interstellar medium radiation flux and traditionally known as the 'Habing flux' (Habing 1968); θ is the azimuthal angle in a spherical coordinate.

2.6. Classification of the initial condition of a cloud

Lefloch & Lazareff (1994) classified the initial physical properties of a cloud and UV radiation field in a two dimensional parameter space (Δ,Γ), which are defined by the following equations(Lefloch & Lazareff 1994),

$$\Delta=\frac{n_i}{n_0}=\frac{c_i}{2\eta\alpha_B n_0 R}\{-1+\sqrt{1+\frac{4\eta\alpha_B R J_0(Lyman)}{c_i^2}}\} \tag{17}$$

$$\Gamma=\frac{\eta\alpha_B n_i R}{c_i}=\frac{1}{2}\{-1+\sqrt{1+\frac{4\eta\alpha_B R J_0(Lyman)}{c_i^2}}\} \tag{18}$$

where Δ relates the overpressure of the ionised gas to the undisturbed neutral gas and Γ is the ratio of recombination rate to the ionisation rate, $n_i=xn=n_e$ is the ionised gas density around the cloud, n_0 is the initial density of the hydrogen in the cloud. $\eta\approx0.2$ is a parameter to describe the effective thickness of the recombination layer around the molecular cloud and $c_i=\sqrt{\mathcal{R}T_*}$ is the isothermal sound speed in the ionised gas with $\mathcal{R}$ being the gas constant. The 2-D parameter space can be divided into five different regions according to the effect of the UV radiation on the evolution of a cloud.

Region I is defined by $\frac{\Gamma}{\Delta}\leq1.4\times10^{-2}$, where the opacity of the cloud is very low ($\ll1$) so that it is initially transparent to the UV radiation. Region II is defined by $\Delta\leq\frac{c_n^2}{2c_i^2}\sim10^{-2}-10^{-3}$ with $c_n=\sqrt{\mathcal{R}T_n}$ being the isothermal sound speed in the neutral gas of temperature T_n, in which the effect of the ionisation is too weak to produce any noticeable dynamical effect. Therefore clouds starting in region I and II are too trivial to be discussed.

On the other end, when Δ is high, i.e., $2\leq\Delta\leq\sqrt{10}$, which defines the region III, the cloud is entirely photo-ionised in an ionisation flash by Lefloch's model in which the self-gravity of the cloud is not taken into account. Region IV is defined by $\Delta<\frac{J_0(Lyman)}{n_0c_i(1+\Gamma)}$,

where the whole dynamical evolution of the cloud will be governed by the propagation of a D type ionisation front preceded by an isothermal shock in the cloud. Finally $\Delta > \frac{J_0(Lyman)}{n_0 c_i(1+\Gamma)}$ defines the region V, where an initial weak R ionisation front would gradually become a D type ionisation front propagating toward the interior of the cloud.

For the clouds starting in regions III - V, although the detailed evolutionary features of the cloud can only be obtained through the numerical simulations described above, an existing simplified analytical result derived by Kahn (1969) could help astronomers predict the final evolution of the globule under observation and also provides us a way to validate our numerical results. Therefore we briefly present it in the following subsection.

3. A preview: A simplified analytical result

In the simplified analytical result, only the effect of UV component is considered since it is much stronger than FUV radiation as given in section 2.5. The viscosity term in Equation (2) will be neglected because of its smaller magnitude than the other terms.

After an initial ionising stage by the UV radiation flux, the stream of the ionised hydrogen forms a warm halo around the globule which has a radius r_i, at which the globule is bounded by an ionisation front while an isothermal shock propagates toward the interior of the globule. Assuming a steady ionised gas flow from the surface of the globule which can be approximated as a spherical isothermal sphere and a balanced ionisation-recombination in the halo, Kahn (1969) derived a necessary condition for the globule to be stable against the gravitational collapse. Based on the analytical solutions of Equation (1-2) in the ionised gas halo and in the neutral globule, this critical condition is expressed by the current mass of the neutral globule

$$M \leq M_{max} = 1.29\left(\frac{\alpha_B c_n^{14}}{16\pi^2 m_H^2 c_i^4 J_0(\mathrm{L}yman) G^5}\right)^{1/3} \tag{19}$$

where G is the gravitational constant.

The importance of this result is that the quantities such as $T_n(c_n)$, $T_i(c_i)$ and J_0(Lyman) can be estimated by the observational data, then Equation(19) can be used to estimate the maximum mass for the globule to contain in order not to go collapse if the structures of both the globule and halo can be regarded as steady. On the other hand if the current mass M of the globule derived from the observational data is higher than M_{max}, the globule under the investigation would finally collapse to form new star at the end of the evolution, vice verse, the globule may stay stable until it is completely evaporated by the UV radiation. The advantage of the Equation(19) is that the criteria for globule's stability is in terms of

the current mass of the globule instead of the initial mass of the cloud, the latter is hardly known by observations.

In the following, we will discuss the detailed evolutionary features of clouds, based on the numerical simulations. In this paper we will mainly study the morphological evolution of BRCs and try to find solutions for the questions raised in the beginning of the paper. A systematic investigation on the ionisation radiation triggered star formation in BRCs will be presented in our next paper.

4. Results and discussions

The most important difference between our newly developed RDI model and Lefloch's model is the inclusion of the self-gravity of a molecular cloud, therefore we will firstly investigate the role of the self-gravity of a molecular cloud in its dynamical evolution when it is under the effect of UV radiations, so that we can explore the possibility to relax the extreme zero velocity boundary condition in order to derive the predominance of type A BRCs, and discuss the possible modification to the classification of Lefloch's 2-D parameter space caused by the inclusion of the self-gravity of the molecular cloud.

We then will explore the effects of initial thermal state of a cloud, the strength of UV radiation flux, and also initial turbulent state (non-thermal motion) on the morphological evolution of molecular clouds.

The molecular cloud is presented by 20,000 SPH particles. In the following analysis to the numerical results, we will concentrate on the effect of the UV radiation falling onto the surface of the front hemisphere, since the heating effect of photoelectric emission of electrons from dust grains by the isotropic FUV radiation is much weaker than that of hydrogen ionisation by Lyman continuum radiation which only affects those gas particles at the front surface layer.

4.1. The effect of initial self-gravity of a molecular cloud

The gravitational potential energy of a spherically uniform molecular cloud of mass M and radius R is $\Omega = -\frac{3GM^2}{5R}$. In order to explore the role of the initial self-gravity of a molecular cloud in its morphological evolution, we perform two different sets of simulations, one set of the three clouds having a same mass of $35M_{\odot}$ but different radii, the other having a same radius of 0.5 pc but different masses. Therefore our simulations cover different cases in which the initial self-gravity of a molecular cloud changes.

The initial temperature of the molecular clouds is all set to 60 K. These chosen initial conditions guarantee that the simulated molecular cloud will not collapse by self-gravity if there is no external radiations.

4.1.1. Clouds with a fixed mass of 35 $M_\odot$

Due to the change of the radii of clouds, the initial ionisation/recombination states change as well. The first six columns in Table 1. list the parameters of the first set clouds called A, B, C and their initial locations in the (Δ, Γ) parameter space respectively. The features of cloud D in the list will be discussed later. The ratio of the initial gravitational energy of the three cloud A, B, and C is $\Omega_A : \Omega_B : \Omega_C = 1 : 0.38 : 0.26$ and the ratio of gravitational forces of the clouds A, B and C onto a mass element at their surfaces are correspondingly $F_A : F_B : F_C = 1 : 0.14 : 0.07$, which defines significantly different initial self-gravity in the three molecular clouds.

According to Lefloch's model, cloud A would evolve into a cometary globule after passing a morphological sequence from type A to type B then to type C, and finally it will be completely evaporated in a few Mys, while cloud B and C would be evaporated in a so called 'ionisation flash'. It is our interest to see how these clouds would evolve differently if the self-gravity of a cloud is taken into account.

I: CLOUD A

The images in Figure 2 reveal the morphological evolution of cloud A by number density of hydrogen nuclei and the line plots in Figure 3 describe how the UV radiation induced shock front leads the ionisation front propagating into the interior of the cloud and finally results in the collapse of the cloud. Figure 4 is the corresponding velocity field evolution diagram, which gives the kinematic explanation on the formation of the morphologies of the cloud at different evolutionary stages.

The image in the top-left panel of Figure 2 and the solid line in the top-left panel of Figure 3 show the number density distribution of cloud A at an early stage ($t = 700$ years). It is seen that the density profile of the whole cloud has not yet changed much from the initial uniform distribution. The top-left panel in Figure 4 shows a rather random velocity distribution which is very similar to the initial random velocity distribution of the cloud.

However the dashed line in the top-left panel of Figure 3 tells that an ionisation front has been built up at the front surface of the upper hemisphere of the cloud after the intensive Lyman continuum flux falls onto the front surface. The gas in the top layer is fully ionised

($x \sim 1$) and the resulted ionisation heating rises its temperature to 10^4K. When $t = 0.2 \times 10^5$ years, the ionised gas at the front surface of the cloud evaporate radially away from the front surface as shown by the velocity profile in the middle panel of Figure 4 and by the furry gas above the front surface in the top-middle panel of Figure 2. The falling tail beyond $z = 0.4$pc in the solid line of top-middle panel in Figure 3 shows that the density of the evaporated gas is about 100 cm^{-3}.

On the other hand, the high temperature in the front top layer produces a high pressure, i.e., an isothermal shock driven into the cloud. The neutral gas ahead the shock front is then compressed. The contour lines around the front surface layer of the cloud in the top-middle panel in Figure 2 and the small peak (if we define it as the shock front) around $z = 0.4$pc in the solid line of the top-middle panel in Figure 3 show that a density gradient starts to built up as a consequence of the shock compression.

The UV radiation induced shock velocity $v_c(\theta)$ at the front surface is approximately given by Lefloch & Lazareff (1994),

$$V_c(\theta) = V_c(0)(cos(\theta))^{1/4} \tag{20}$$

where θ is the angle of a surface point from z axis and $0 \leq \theta \leq \pi/2$ as shown in Figure 1; $V_c(0)$ is the shock velocity at the the point $r = R, \theta = 0$ and $V_c(0) \sim [J_0(\text{Lyman})/n]^{1/2}$ (Bertoldi 1989). The direction of V_c is along the normal of the point (R,θ). The resulted velocity distribution $V_c(\theta)$ in the shocked gas is obviously seen in the top-middle panel of Figure 4.

At time $t = 2.0 \times 10^5$ years, the shock front leads the ionisation front moving toward the rear hemisphere as shown by the solid and dashed lines in the top-right panel of Figure 3. The ionisation ratio x has decreased a lot in the shocked part of the cloud, because the recombinations of electrons with their parent ions in the surrounding envelop have consumed most of Lyman photons. On the other hand the shocked gas at the front surface around $\theta \sim 0$ have the highest V_c so it moves faster toward the rear hemisphere than that in the peripheral part of the compressed layer. Consequently, the faster progression of the central parts of the compressed layer at the front surface causes a deviation of the morphology of the front surface from a hemisphere, i.e, the front surface of the hemisphere becomes seriously squashed so that a type A rim forms, which can been seen from the top-right and the subsequent panels of Figure 2.

At the same time, the strongest compression of the gas located at $\theta \sim 0$ forms a small but highly condensed core at the head of the front hemisphere, shown as in the top-right panels of Figures 2 and 3, which creates a new gravitational centre G to its surrounding gas particles so that the latter gain an acceleration a_G hence a velocity component V_G as shown

in Figure 5. The surrounding gas then gradually collapse toward the core centred at G, as shown in the panels from the top-right to the bottom-right panels in Figures 3 and 4.

Due to the distortion of the front surface, the velocity of the shocked gas in the outermost parts of the front hemisphere ($\theta \sim \pi/2$) is significantly changed so that its trajectory intersects the rear edge of the original cloud to form the 'ear-like' structures as shown by the two convex parts at $\theta \sim \pi/2$ in the top-right and bottom-left panels of Figure 2.

As illustrated in Figure 5, the total velocity V_T of the gas particle at the sample point in the 'ear-like' structure directs to the C' point on the z axis, instead of C point, which would be the converging point if the self-gravity of the globule was not taken into account. Hence the 'ear-like' structures converges to z axis to form a tail structure which overshoots the rear surface of the cloud and is well described by the solid line beyond $z < -0.5$pc from the top-right to bottom-right panels of Figures 3 and 4.

At $t = 0.351$ My, the type A BRC structure comes to a thermally quasi-static state (with a pressure $P/k \sim 10^6$ Kcm^{-3} close to the boundary between the neutral gas and the ionised envelop) after an initial drastic and transient evolutionary period. As shown in Figure 3, the whole structure has shown the typical stratification of an observed BRC (Lefloch et al 2002) from the centre to outside:

i) An isothermal neutral core of a radius of 0.15 pc ($-0.3 < z < 0$ pc) with a central density of a few 10^5 cm^{-3} and an average temperature of $T_n = 28$ K

ii) A very thin layer of PDR (Photon-Dominated Region: $0 < z < 0.05$ pc) with an average density 10^4 cm^{-3}, an temperature ~ 1000 K and an electron density $n_e < 10$ cm^{-3} with the ionisation fraction $10^{-5} < x < 10^{-3}$.

The mass included in the isothermal core including the PDR (with density from 10^4 to a few 10^5 cm^{-3} as observed) is 15 M$_\odot$.

iii) A photoionised envelope (Bright rim: $0.05 < z < 0.11$pc), the density drops sharply from a few 10^3 to a few 10 cm^{-3} and the ionisation ratio $10^{-3} < x \leq 1$, i.e., n_e distribution between 10 and 10^3cm^{-3}. The average temperature T_i is about 10^3 K.

iv) The evaporated ionised tenuous gas into the HII region ($z > 0.11$pc) with an average density a few 10 cm^{-3} and $x = 1$, but a very high average temperature of 5×10^4 K.

Now the most concerned question on its further evolution is that whether the whole globule is stable against the gravitational collapse or not. Before revealing the numerical solution to this question, we can employ Kahn's analytical result to predict this globule's final evolution and then use the result to validate the numerical solution. Substituting all of

the values into Equation (19), we obtain the maximum mass for the isothermal core to be stable is $M_{max} = 3$ $M_\odot$. Therefore this type A BRC should finally collapse since the current mass of the core is 15 $M_\odot$, much higher than M_{max}.

The numerical results after $t = 0.35$ My as shown by the bottom middle/right panels in Figures 2, 3 and 4 reveal that the globule quickly collapse toward its G centre under the effect of the enhanced self-gravity. The central density of the core reached 2×10^8cm^{-3} when $t = 0.391$My and 5×10^{10} cm^{-3} when $t = 0.394$My. Therefore we could conclude that the radiation triggered star formation in cloud A is expected to occur because the central density has reached such a high value (Nelson & Langer 1999), which is consistent with the analytical result.

II: CLOUD B

The morphological evolution of cloud B is shown in Figure 6, while Figure 7 describes how the shock front leads the ionisation front propagating into the cloud and Figure 8 displays the corresponding evolutionary sequence of its velocity field.

During the first 0.4 My, the main characteristics of the morphological evolution of cloud B are similar to that of the cloud A. The gas particles at the top layer of the front hemisphere are continuously ionised, evaporated and form a hot photo-ionised envelope around the type A rim at the front surface of the globule. On the other hand, the radiation induced shock leading an ionisation front propagates into the cloud and compresses the neutral gas ahead to form a condensed core.

However the morphological evolution of cloud B starts to show obviously different feature at $t = 0.63$My. It is seen from the bottom-left panel of Figures 6 that the front surface becomes a type B rim with a dense core behind the rim. Also a more extensive tail than that in cloud A is formed by the gas particles from the 'ear-like' structure converging to z axis as shown by the solid lines beyond $z < -1$ pc in the bottom panels of Figure 7. We will discuss the kinematics which make the difference in the morphological evolutions between cloud A and cloud B after the presentation of the evolutionary features of cloud C.

Around the front hemisphere of the type B BRC, a similar thermally quasi-stable stratification to that of cloud A at $t = 0.351$ My is formed with an isothermal condensed core of a radius of 0.2 pc at the head of the globule as shown in the bottom-left panel of Figure 7. The core has a central density slightly lower than 10^5 cm^{-3}, and an average temperature $T_n = 31$ K, which is surrounded by a thin layer of photo-ionised envelope of a temperature $T_i = 10^3$ K. The core including the PDR contains a mass about 13.5 $M_\odot$ which is higher than the M_{max} =3.6 $M_\odot$ given by Equation(19). Therefore the core should be expected to collapse. The simulation results presented in the bottom middle/right panels of Figure 6 and

Figure 7 show that the core continuously gets denser, and the central density has reached a few $\times 10^5$ cm^{-3} at $t = 0.79$ My and a few $\times 10^{10}$ cm^{-3} at $t = 0.81$ My, the sign of the triggered star formation which is consistent with the analytical prediction.

III: CLOUD C

The evolutionary sequences of density, ionisation ratio and the velocity field of cloud C are shown in Figures 9, 10 and 11 respectively. In the first 0.86 My, the dynamical evolution of the cloud C displays similar features to that of cloud B. A type A rim firstly forms after $t = 0.365$ My, and then a type B rimmed morphology develops when $t = 0.86$ My, as shown in the corresponding panel in Figure 9. The relevant panel in Figure 10 shows the formation of an isothermal core with a central density slightly lower than 10^5 cm^{-3} and a thin layer of PDR surrounding the core. The average temperature T_n is 35 K in the core and $T_i = 1000$ in the photo-ionised bright layer. The thermal pressure P/k in the different regions is $\sim 10^6$. The mass included within the isothermal core (PDR included) is 11.1 $M_\odot$, which is higher than the 5 $M_\odot$ estimated by Equation (19) Therefore, the core would collapse finally.

However, the gas particles at the two sides of the rear hemisphere continue their movement to z axis to form a longer tail as shown in the bottom-middle panels of Figures 9 and 11 so that the morphology of the globule becomes a type C BRC at $t = 1.034$ My.

The last two panels in Figure 10 shows that the gas particles in the core region collapse to the G centre, so the central density reaches to 10^9 cm^{-3}, which means the beginning of the triggered star formation at $t = 1.12$ My.

In table 1. the final morphologies of the simulated clouds are list in the 7th column and the 8th and 9th columns are the isothermal Core Formation Time (C.F.T.) and the Core Collapse Time(C.C.T.) respectively.

In order to find the mechanism responsible for the differences in the morphological evolution of cloud A, B and C, a further investigation on the kinematics of the shocked gas in the front hemisphere is carried in the following part of the paper.

IV: The Kinematics of morphological evolution

Figure 5 shows that the direction of the total velocity V_T of the shocked gas particles within two 'ear-like' structures determines their converging points on the z axis, hence the length of the tail or say it is the magnitudes of V_C and V_G which determine the morphological evolution of a BRC.

The ratio of the gravitational accelerations of cloud A, B and C on the gas particles in the 'ear-like' structure is $a_A : a_B : a_C = 1 : 0.14 : 0.07$. Hence the relevant velocity

components obey the inequality $V_G(A) > V_G(B) > V_G(C)$. On the other hand, as stated in Equation(20), we have $V_C(\theta) \propto V_C(0) \sim n^{-1/2}$ for fixed J_0 and θ, hence for the particles in the the 'ear-like' structures in cloud A, B and C, the velocity component V_C follows $V_C(A) < V_C(B) < V_C(C)$. Now it is not difficult to understand that the angle δ of a gas particle in the 'ear-like' structure in cloud A, B, C obeys the inequality: $\delta(A) > \delta(B) > \delta(C)$. The distance d between the converging point C' and the new gravitational centre G in clouds A, B and C obeys $d_A < d_B < d_C$, therefore the three clouds evolved to type A, B, and C BRCs respectively.

On the other hand, the escape velocity of a particle at the surface of a cloud is $v_{es} = \sqrt{\frac{2GM}{R}}$. The ratio of the escaping velocities of three clouds is $v_{A(es)} : v_{B(es)} : v_{C(es)} = 1 : 0.37 : 0.26$. The easiness for the mass particles at the surface of the cloud to be photo-evaporated is in the order of cloud C, B, and A, which explains why the masses left in the isothermal cores are 11.1, 13.5 and 15 $M_\odot$ for clouds C, B, and A respectively.

V: Further increment of the radius

We further increase the initial radius of the molecular cloud so that the cloud is initially much less gravitationally bounded than cloud C. The basic features in the evolutionary sequences of the molecular clouds are not much different from that of the cloud C if $R < 4.7$ pc except that both the mass accumulated in the head of the quasi-stable globules and the central density decrease with the initial radius increasing from 1.9 to 4.7 pc.

However when the initial radius increases to $R = 4.7$ pc (the cloud is called cloud D in Table 1), the initial gravitational force to the surrounding gas particles is only about 1.1% of that of cloud A. Cloud D quickly evolves from type A to B then into a loose type C BRC – a cometary globule with a slightly compressed core of a central density of a few 10^2 cm^{-3} when $t = 0.8$ My. Shortly after a weak shock passed the centre of the head, the whole globule undergoes a quick re-expansion and is totally photoevaporated after 1 My in a so called 'ionising flush' (Lefloch & Lazareff 1994).

The above set of simulations prove that changing the initial size of the cloud hence the initial self-gravity could dramatically change the cloud's evolutionary sequence and the final morphology. The result means the initial self-gravity of the cloud plays a dominant role in the morphological evolutions of BRCs. However, changing of the initial self-gravity of the cloud by changing its initial radius creates a second effect at the same time - the alteration of its initial ionisation/recombination state, as shown in Table 1. Hence our confidence in the role played by the self-gravity in determining the morphological evolution of BRCs needs further assurance. The second set of simulations therefore is designed to change the initial density of the cloud by changing its initial mass so that the change in the initial self-gravity

will not bring drastic change in the ionisation/recombination state as shown in Table 2. Hence the role of the self-gravity in the morphological evolution of the BRCs can be further explored.

4.1.2. Clouds with a fixed radius of 0.5pc

Table 2. lists the parameters of the second set clouds called A, A$^{'}$, A$^{''}$ respectively with their initial locations in (Δ, Γ) parameter space and the information on their morphological evolutions.

For cloud A, the evolutionary features has been fully discussed before. and are re-listed in Table 2 for comparison. With the decrement of the initial mass of the cloud, the density of the cloud decreases accordingly, the morphological evolution follows a similar pattern to that in the first set of clouds. The dynamical evolutions of the formation of type A, B and C BRCs exhibit similar sequences to that in the first set clouds. Therefore in order to save space, we don't present the sequential figures on their dynamical evolutions as we did for set one clouds, but only provide a summary on the relevant key features which are partly listed in the Table 2.

When the initial mass of a cloud decreased to 12 $M_{\odot}$, cloud A$^{'}$ evolved from type A to B morphology in a very similar way to cloud B in set one simulation. An isothermal core formed in 0.42 My, and collapsed in 0.8 My, with the central density up to $10^8 \mathrm{cm}^{-3}$ and a final mass of 6.9 $M_{\odot}$ in a collapsed core of 0.1 pc in radius. When the initial mass further decreased to 8 $M_{\odot}$, cloud A$^{''}$ evolved through a sequence of from type A to B then to C morphologies, with formation of an isothermal core at $t = 0.53$ My, which collapsed in 1.5 My with a central density of $10^7 \mathrm{cm}^{-3}$ and a mass of 4.5 $M_{\odot}$ in a core of radius of 0.1 pc.

Finally when the initial cloud mass further decreased to 1 $M_{\odot}$, cloud A$^{'''}$ evolved quickly through type A and B morphologies with a condensed core of a central density of 10^4 cm^{-3}. After evolving to a cometary globule morphology at t = 0.3 My, it re-expands and then is totally evaporated when t = 0.9 My.

In the second set simulations, the initial recombination parameter Γ is same for cloud A, A$^{'}$ and A$^{''}$ because they have same radius. The ratio of the initial ionisation parameters $\Delta(A) : \Delta(A') : \Delta(A'') = 1 : 2.85 : 4$, i.e., cloud A$^{''}$ has the highest value of Δ which is 4 times the lowest value for cloud A. On the other hand, the ratio of the initial gravitational energies of the three clouds is $\Omega_A : \Omega_{A'} : \Omega_{A''} = 1 : 0.12 : 0.052$. The highest value of the initial self-gravitational energy of cloud A is about 20 times of the lowest value for cloud A$^{''}$. It is obvious the difference in the initial self-gravitational energies among the three clouds

is much more distinctive than the difference in their initial ionisation states. Therefore, we can safely conclude that the different morphological evolutions of the three clouds are caused by their different initial self-gravitational states. The role of the initial self-gravity in determining the morphological evolutions of the BRCs is further confirmed.

4.1.3. The Possible modification of the (Δ, Γ) parameter space

From the morphological evolution paths of the 7 clouds, we see that for clouds starting from region V such as cloud A and A', their dynamical evolutions are driven initially by a weak-R ionisation front which quickly changes into a D-type ionisation front, just as what Lefloch described.

However for clouds starting from region III such as cloud B,C,and A", they are not at all entirely photo-ionised by an R-weak front and permeated by an ionisation flash like what Lefloch & Lazareff (1994) described, their dynamical evolutions are driven by a similar mechanism to that of cloud A and A'.

For clouds A$'''$ and D, which also start from region III but with a high initial ionisation state $\Delta \geq 23$, its dynamical evolution is driven by a weak R-front and the whole structure get permeated by an ionisation flash and evaporated quickly just as what Lefloch & Lazareff (1994) described for region III cloud.

Hence it is clear that in term of the dynamical classification of (Δ, Γ) parameter space, the boundary for region III has been pushed greatly from $\Delta < \sqrt{10}$ to $\Delta < 23$ due to the inclusion of the self-gravity of the cloud.

4.1.4. Zero self-gravity and surface instability of the cloud

In order to further support our argument on the role of self-gravity of the cloud in the morphologic evolution process, we take off the self-gravity of the three clouds A, B and C and re-run the simulations. The result reveals very similar evolutionary sequence to that of Lefloch & Lazareff (1994). The evolutionary sequence passes type A to B morphologies and then form a type C BRC. Then it re-expands and finally totally evaporated between 1 to 2 My.

To some stage of the evolution of the molecular cloud, the ionisation flux onto the front surface of the cloud is perturbed somehow due to the recombinations of the electrons onto the ionic atoms, which causes instability of the front surface of the cloud as described in

the lefloch's simulations (Lefloch & Lazareff 1994). We found from our simulations that the scale of the instability is closely related to the initial ionisation state of the cloud. For all of the 7 clouds we simulated, except cloud D, their initial ionisation state are not very high when compared to that of the cloud D, very small scale perturbations (with wavelength $\lambda < 0.2R << R$)) at the front surface appeared, as seen from the up-middle panels of Fig.2, 6 and 9, but they are quickly smoothed out.

For cloud D, due to its extremely high initial ionisation state, the surrounding of the front surface quickly becomes recombination dominant region, so large scale perturbations (with wavelength $0.2R < \lambda < R$) grow at $t = 0.06$ My from the front surface of the cloud which can be seen from the up-left panel of Figure 12. However the large scale perturbation is stable because it is gradually smoothed out with the core further being compressed by the isothermal shock. At $t = 0.8$ My, the front surface becomes very smoothed. We think it is the gradually increased gravity from the core underneath the front surface which suppressed further growth of the surface instability.

We conclude that with inclusion of the self-gravity in the model, both small and large scale surface instabilities caused by the perturbation to the ionisation flux are stable and will be smoothed out over the further evolution of the cloud. Our conclusion is in agreement with what revealed by Kessel-Deynet & Burkert (2003) in Case B in their paper on the stability of the front surface of the cloud.

We have shown that the self-gravity indeed plays an important role in the morphological evolution of the molecular clouds. For any change in the initial conditions of a cloud, if it greatly results in a change in its initial self-gravitational state, the cloud will alter its morphological evolution.

4.2. Initially Thermally Supported Clouds

In order to see how the three clouds would evolve if they are only initially thermally supported, i.e., if the cloud A, B and C start their evolutions without the initial turbulence. We re-run the simulations for cloud A, B and C respectively by setting a zero initial velocity field to each of them. Since the general features of the morphological evolutions of the three molecular clouds are qualitatively similar to that presented in last section, we mainly describe the different features in their evolutions.

Cloud A evolved into a type A BRC with a condensed core of a central density of a few $10^8 \mathrm{cm}^{-3}$ within 0.37 My. Cloud B evolved into a type B BRC with a condensed core of a central density $10^9 \mathrm{cm}^{-3}$ within 0.74 My. Cloud C reached a type C BRC structure with a

core density of $10^9 \mathrm{cm}^{-3}$ within 0.98 My. Compared with the corresponding results in Section 4.1.1, the clouds without initial turbulence take less time to collapse. Further comparing the velocity field evolutions of the two group molecular clouds, we find the initially turbulent field takes 0.02 My in cloud A, 0.07 My in cloud B and 0.14 My in cloud C to dissipate, which shows the initially turbulent clouds is just delayed to form a highly condensed core. Therefore we conclude that the initial turbulence does not effect a cloud's final morphology type. The results is consistent with that of an investigation by Nelson & Langer (1999) on the dynamical evolutions of Bok globules affected by FUV radiation.

4.3. Effect of changing initial density profiles

All of the above simulations are based on an initially gravitationally stable and uniform cloud. Although large degrees of central condensation should not be expected in the initially gravitationally stable molecular cloud, we are still interested in examining the effect of the initial central condensation of a molecular cloud on its morphological evolution. The following initial density distribution is used,

$$n(r) = \begin{cases} n_0 \ (0 \leq r \leq r_0) \\ n_0(\frac{r_0}{r})^2 \ (r_0 < r \leq R) \end{cases}$$

which represents for a condensed uniform core with a radius of r_0 and density of n_0 surrounded by an envelop of a density profile proportional to r^{-2}. For a given r_0, R and M, n_0 can be found from the equation $4\pi m_H \int_0^R n(r) r^2 dr = M$.

When we start with $r_0 = 0.5R$, the evolutionary sequences of clouds A, B and C with an initial core-halo mass distribution do not show significant change from that of initially uniform clouds. The basic features of type A, B and C are kept, except that the main body of the formed BRC structure are all smaller than that formed in initially uniform clouds. Then we decrease the radius of the central condensation to $r_0 = 0.2R$, the morphological evolution show obvious changes. Cloud A ends its evolution in type B as shown in Figure 13, and cloud B in type C as shown in Figure 14, while cloud C developed into a very narrow shaped type C at a much early time ($t = 0.67$ My) as shown in Figure 15. Their morphologies are all elongated than that of their corresponding uniform clouds. This morphological change can be well explained by the illustration in Figure (5), the gas particles in the halo has a lower density therefore a higher V_C component, which makes them converge to a farther point C' from point G on the z axis.

The mass left at the collapsed core of 0.15 pc in cloud A, B, and C are 10.5, 7.2, 5.6 $\mathrm{M}_\odot$ respectively, which are less than that in their corresponding initially uniform clouds. This is

because the density in the initial halo of a cloud is lower than that in the same part of the initially uniform cloud hence the halo in the front hemisphere is at a higher initial ionisation state, in which particles are easier to be ionised and then to be photo-evaporated.

In summary, the initial mass condensation state does affect a cloud's morphological evolutions because it changes the initial self-gravitational state of a cloud.

4.4. Effects of the boundary conditions

As stated in Section 2.5, we apply a constant pressure boundary condition, which resembles the physical conditions of a very hot HII region. In order to examine the effect of the boundary condition on the dynamical evolution of a cloud we decrease the value of the surrounding pressure P_{ext}/k to mimic a less violent environment. For each of three clouds in the first set, we re-run the simulation for two different values of the external pressure, i) $P_{ext}/k = 10^3$ Kcm^{-3} which corresponds to a warm interstellar medium environment (Nelson & Langer 1999) and ii) $P_{ext}/k = 0$ which describes a vacuum environment so that the ionised gas is able to freely expand from the surface of the cloud.

It is found that with decreasing external pressure, although cloud A still evolves to a type A BRCs under the boundary condition i) and ii), the curvature of the front surface increases and the shape of the final condensed core becomes elongated. Cloud B with boundary condition i) evolves to a slightly elongated type B BRC but evolves to a type C BRC at $t = 1.6$ My under the boundary condition ii), as shown in Figure 16. Cloud C forms a type C BRC in both cases, but the length of the tail increases with the decrease of the external pressure. It is obvious that the lower pressure environment favours formation of morphology with higher curvature, or high pressure environment favours formation of type A BRCs. The conclusion is consistent with that of zero velocity boundary condition (Lefloch & Lazareff 1994).

4.5. The effect of initial temperature of molecular clouds

According to observations, the temperatures of molecular clouds are generally in the range of $10 - 100$ K (Bertoldi 1989). We then carried out two more sets of simulations for each of the three molecular clouds A, B and C with the initial temperatures $T_1 = 20$ K and $T_2 = 100$ K respectively, while all of the others physical conditions are kept the same as that in Section 4.1.1.

The evolutionary sequence of each simulation is qualitatively similar to its corresponding cloud with an initial temperature of 60 K.

When the initial temperature $T_1 = 20$ K, the evolutionary sequences of cloud A, B and C basically exhibit no significant differences from that described in Section 4.1.1. Cloud A evolves to a quasi-stable type A rimmed morphology with a condensed core at the head of its front hemisphere. The central density of the core reaches a value of 10^9 cm^{-3} in 0.37 My when it finally collapses. Cloud B evolves from type A to B morphology with a condensed core at the head of its front hemisphere in 0.6 My and the core reaches a central density of 10^{10} cm^{-3} at $t = 0.79$ My. Similarly cloud C evolves to a type C BRC after passing type A and B morphologies. It collapse at $t = 1.01$ My when the central density of the core is 2×10^9 cm^{-3}.

When the initial temperature rises to 100 K, cloud A still evolves to a type A rimmed morphology having a condensed core which collapses after the central density is up to a few 10^8 cm^{-3} in the front hemisphere at $t = 0.42$ My. Cloud B evolves to a type B rimmed morphology and the condensed core collapse with the central density being up to 10^9 cm^{-3} at $t = 0.93$ My. Cloud C evolves to a type C rimmed BRC plus a small core of centre density of 10^9 cm^{-3} in 1.32 My.

In summary, the variation of the initial temperature of molecular clouds between 10 - 100 K does not significantly change the morphological evolution of a cloud, which is physically understandable since the thermal pressure of a cloud is not important in the dynamical evolution in BRCs (Bertoldi 1989; Lefloch & Lazareff 1994; White et al. 1999). Higher initial temperature in a cloud delays its collapsing time, for the initial thermal motions of gas particles dissipate over a period of time. The morphological evolution of a cloud is mainly decided by the dynamical behaviour of the gas particles within the two sides of the cloud ($\theta \sim \pi/2$), which is largely dependent on the strength of the ionising flux and the self-gravity of the cloud as shown in Section 4.1.

However, the initial temperature of a cloud does affect the amount of mass condensed in the core of a BRC, for which we will have a detailed discussion when we study the UV radiation triggered star formation in BRCs in our next paper.

4.6. The effect of the strength of ionising flux

We also carried out a set of simulations on the influence of the strength of an ionising flux on the evolutionary process of BRCs. The change in the strength of ionising flux incident on the front surface of a molecular cloud corresponds to two different cases: i) a cloud can be at different distances from an ionising star; ii) an ionising star in different types radiates with different flux strength. This set of simulations is to see whether the molecular clouds within

one giant cloud cluster would exhibit essential difference in their morphological evolutions due to their different distances from the central star.

Since the ionising flux $J(\text{Lyman}) \propto 1/D^2$, where D is the distance of a cloud from the ionising star. For each of cloud A, B and C, we re-run the simulations twice by setting two different J(Lyman) flux values. If we assume cloud A, B and C in Section 4.1.1 are in a distance of D_0 from the ionising star, then $J_1(\text{Lyman}) = J_0(\text{Lyman})/4$ means we move the star twice distance away, i.e., $D = 2D_0$. If we set $J_2(\text{Lyman}) = 4 \times J_0(\text{Lyman})$ which means the original cloud is moved to half distance closer, i.e, $D = D_0/2$. The spatial range of 0.5 - 2 D_0 from the ionising star should be large enough to include most molecular clouds in one cloud cluster.

The simulation results revealed that for all of the three molecular cloud A, B, and C, their morphological evolutions are not very sensitive to the strength of the ionising flux in the above specified range and they follow very similar evolutionary sequences to that when ionising flux is $J_0(Lyman)$.

The result looks a bit puzzling at the first glance, since the velocity component V_C of the ionised gas in the top layer of the cloud increases with the ionising flux, as shown in Figure 5, so that we should expect the angle δ decreases with the ionising flux, which will favour the formation of type C rim morphology. However, if we consider the effect of the enhanced shock effect due to increased ionising flux, the compression to the core in the front hemisphere will be stronger. Therefore the core will exert a stronger attractive force on its peripheral gas particles which then results in a higher V_G so that angle δ of the velocity remains basically unchanged although the magnitude of the total velocity may increase, which would decrease the time needed for the gas particles in the ear-like structures to collapse onto the symmetrical axis. The same consideration can explain the insensitivity of the morphological evolution of the cloud to the decreased radiation flux and the time needed for the gas particles to collapse onto the symmetrical axis is found to be elongated.

4.7. Confrontation with observations

The simulations on a set of molecular clouds reveal that the morphological evolution of a molecular cloud under the effect of the UV radiation does not necessarily go through all of the three morphologies and then end up at cometary type C morphology as described by the previous models. Depending on its initial gravitational state, a cloud could evolve to any one of the three type BRCs. The diversity of the evolutionary sequence of BRCs revealed from our modelling provides a good prospect for us to explore the possible explanations for the

questions raised from BRCs' observations and presented in the introduction of this paper.

The modelling results for the molecular cloud A, B, C under the same initial temperature and ionising flux tell us that the evolutionary paths of all molecular clouds would firstly pass the type A morphology. However some of molecular clouds would only evolve to a quasi-equilibrium type A morphology plus a highly condensed core at the head of its front hemisphere, if their initial self-gravitational energy is high enough. Therefore we shall statistically be able to observe many more type A BRCs than type B or C BRCs in a random observation.

Our modelling results also shows that the UV radiation triggered collapse of a cloud onto the centre core in its front hemisphere could occur with any one of the three morphologies, so it is not surprising at all that the UV radiation triggered star formation occurring in type A BRCs could be observed.

Finally, we come to understand the spacial sequence of type A-B-C BRCs with their distance from the centre star in the Ori OB 1 association (Ogura & Sugitani 1998). We might think this morphological distribution of BRCs as the result of decreasing illuminating flux with distance. However as shown in the argument in Section 4.6, the morphological evolution of the cloud is insensitive to the change of the UV radiation flux in the range discussed. Based on the results derived from the simulations, we can understand this observation from two aspects.

First, we know that where a new star is formed inside a giant molecular cloud as a result of local molecular gas collapse onto a central point, the density of the surrounding gas can be reasonably assumed to decrease with the distance from the central star. It is also known that giant molecular clouds are very clump (Tatematsu et al 1991). Considering the above two points we can assume that the densities of molecular clumps surrounding a new star decrease with their distance D from the central star. If we further assume that the clumps in a giant molecular cloud are of similar radius R, then the initial gravitational potential energy of a clump decrease with their distance from the centre of the star for the gravitational potential energy can be written as $\Omega \sim M^2/R \sim R^5 n^2$, where n is the initial number density of the clumps.

The molecular clumps closest to the central star could possibly evolve to a quasi-equilibrium type A BRC because they have highest initial self-gravitational potential energies, while for those clumps farther away, they evolve from type A to a quasi-equilibrium type B BRC because of their moderate initial self-gravitational potential energies. For those farthest away from the central star, they evolve to pass type A and B morphologies, then to a cometary type C morphology due to their lowest initial self-gravitational potential energies.

Secondly, we already showed in Section 4.4 that at the borders of HII region, type A BRCs are favoured.

Therefore the spatial sequence of type A - B - C BRCs with their distance to the central star can be seen as a manifestation of the mass density distribution of the very clumpy giant molecular clouds.

5. Conclusions

A three dimensional and comprehensive RDI model has been developed with the SPH technique, which self-consistently includes the hydrodynamical evolution, the self-gravity of the cloud, the energy evolution, radiation transferring and a basic chemical network. T The investigation on the morphological evolutions of BRCs are carried out by employing the newly developed model in order to understand a series of puzzles coming from BRCs observations. It is found that the morphological evolution of a molecular cloud is much more sensitive to its initial self-gravitational state than to other physical conditions such as the initial temperature between 20 and 100 K, or the ionising radiation flux within one order of magnitude higher or lower than J_0(Lyman). Our modelling results have revealed that there are three different evolutionary prospects when a molecular cloud is under the effects of ionisation radiations.

For a molecular cloud of an initial mass 35 $M_\odot$ and initial temperature 60 K under the effects of UV and FUV radiation fields specified above, the simulation results revealed: a) if its initial radius is 0.5 pc, it will evolve to a quasi-stable type A BRC; b) when its initial radius increases to 1.3 pc, its evolution will firstly pass a type A morphology and continue its journey to a quasi-stable type B rimmed morphology; c) when the initial radius further increases to 1.9 pc, its evolutionary process follows a sequence of type A→B→C morphologies. d) Further increasing the cloud's radius to 4.7 pc, the evolution of the cloud also follows the sequence of type A →B→C, but the finally formed type C BRC will be totally photoevaporated.

Further simulation results also show that the initial central condensation of the mass in a cloud could change its morphological evolution in term of its initially uniform correspondence. At the border of HII regions, the formation of type A BRCs are favoured. When a molecular cloud is set to a zero initial self-gravitational potential energy or with a low initial density, its morphological evolution sequence is consistent with that by Lefloch's model which is a 2-D model and didn't include the self-gravity of the cloud.

With the knowledge obtained from the modelling, we are now able to confront with the

questions raised by observations. Since all of the clouds evolve to pass a type A morphology and some of the clouds with enough high initial gravitational potential energy would just evolve to a quasi-stable type A morphology, statistically many more type A BRCs should be observed over a random observation. For those BRCs who evolve to a quasi-stable type A rimmed morphology, if the core mass contained in their front hemisphere is high enough for it to collapse, new star could be triggered to form. Star forming signal should be observed. Furthermore if the initial densities of the molecular clumps in Ori OB 1 associations decrease with their distances from the centre of the ionising star, a spacial distribution of type A-B-C BRCs with distance from the central star could exist.

It is obvious that the inclusion of the self-gravitation in our model revealed a diversity of the evolutionary sequence of a molecular cloud under the effects of UV radiations. The satisfactory explanations based on the modelling results to the observational puzzles state that the self-gravity of a molecular cloud indeed plays an important role in controlling the evolutionary destiny of a molecular cloud and should not be neglected especially when we try to achieve a whole picture of the dynamical evolutions of molecular clouds. This is because the radiation induced shock dramatically enhances the effect of the self-gravity of the clouds. Consequently, some modifications on the region classification in Lefloch's parameter space have been confidently derived. The boundary between the D-type ionisation front and 'ionising flush' is extended from $\delta = \sqrt{10}$ to 23 as a result of the inclusion of the self-gravity of the molecular cloud.

REFERENCES

Bertoldi F, 1989, ApJ, 735

Cantó J., Raga A., Steffen W., Shapiro Paul R., 1998, ApJ502, 695

Dyson J.E., Williams D.A., 1997, The physics of the interstellar medium, 2nd Edi.IOP Publishing, Bristol and Philadelphia

Eddington, A.S., The internal constitution of the stars, 1st Edi., Cambridge University Press

Gammie C. F., Ostriker E.C. 1996, ApJ, 466, 814

Goodman A. A., Barranco, J A, Wilner D J, Heyer M H, 1998, ApJ504, 223

Gorti U, Hollenbach D, 2002, ApJ, 573:215-237

Habing, H. 1968, Bull. Astron. Inst. Neth., 19, 421

Hummer D. J. & Seaton M. J. 1963, MNRAS, 125, 437

Jijina J., Myers P.C., Adams F.C., 1999, ApJS, 125, 161

Kahn, F. D., 1969, Physica, 41, 172-189

Karr J.L., Martin, P.G., 2003, ApJ, 595, 900

Kessel-Deynet O. Burkert A., 2000, MNRAS, 315, 713-721.

Kessel-Deynet O. Burkert A., 2003, MNRAS, 338, 545-554.

Klessen Ralf S, Heitsch Fabian, Maclow Mordecai-Mark, ApJ, 2000, 535:887-906

Lee Hsu-Tai, Chen W.P., Zhang Zhi-Wei, Hu Jing-Yao, 2005, ApJ, 624:808-820

Lefloch B, Lazareff, B., 1994, A&A, 289, 559-578

Lefloch B, Cernicharo J, Rodriguez L.F., Miville-Deschenes M.A., Cesarsky D and Heras A., 2002, ApJ, 581:335-356.

Mac Low Mordecai-Mark, Klessen Ralf, Burkert Andreas, 1998, Phys. Rev. Lett. 80, 2754-7

Mac Low Mordecai-Mark, 1999, ApJ, 524:169-178

Miao J, White Glenn J.,Nelson R., Thompson M., Morgan L., 2006, MNRAS, 369, 143-155.

Nelson, Richard P., Langer William D. 1999, ApJ, 524, 923-946

Ogura Katsuo, Sugitani Koji, 1998, Publ. Astron. Soc., 15, 91-8

Oort Jan H., Spitzer L J, 1955, ApJ, 121.

Osterbrock, 1974, D.E., Astrophysics of Gaseous Nebulae, W.H.Freeman and company.

Padoan P., Nordlun A, 1999, ApJ, 526, 279

Raga A C, de Gouveia Dal Pino E M, Noriega-Crespo A, Minimmi P D, Velazquez P F, 2002, A&A, 392,267.

Sugitani K, Fukui Y, Ogura K, 1991, ApJ, 77:59-66.

Sugitani K., Ogura K., 1994, ApJ, 92:163-172.

Tatematsu, K., et al, ApJ, 404, 643

Thompson M.A., Urquhart J.S. White G.J., 2004, A&A, 415, 627-642

Thompson, M.A., White, G.J., Morgan, L.K., Miao, J., Fridlund, C.V.M, Huldtgren White, M. 2004, A&A, 414, 1017-1041

Thompson, M.A., White G.J., 2004, A&A, 419, 599-605

Urquhart, J.S., Thompson, M.A., Morgan, L.M. White, Glenn J. 2006, A&A, 450, 625-643.

Vanhala, Harri A.T., Cameron, A.G.W. 1998, ApJ, 508:291-307

White,Glenn J, Nelson, R. P., Holland W. S., Robson, E. I.; Greaves, J. S., McCaughrean, M. J., Pilbratt, G. L., Balser, D. S., Oka, T., Sakamoto, S., Hasegawa, T 1999, A&A, 342, 233-256

Williams R J R, Ward-Thompson D, Whitworth A P, 2001, MNRAS, 327, 788.

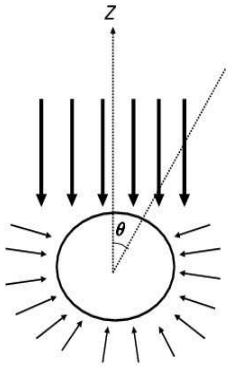

Fig. 1.— The initial geometry of a molecular cloud and the configuration of the radiation fields. The heavy arrow lines above the upper hemisphere represent the sum of the strong UV (Lyman continuum) flux from the massive stars above the molecular cloud and the isotropic FUV flux from the background star radiation and the light arrow lines below the lower hemisphere represent the isotropic FUV radiation ($h\nu < 13.6$ eV) flux only.

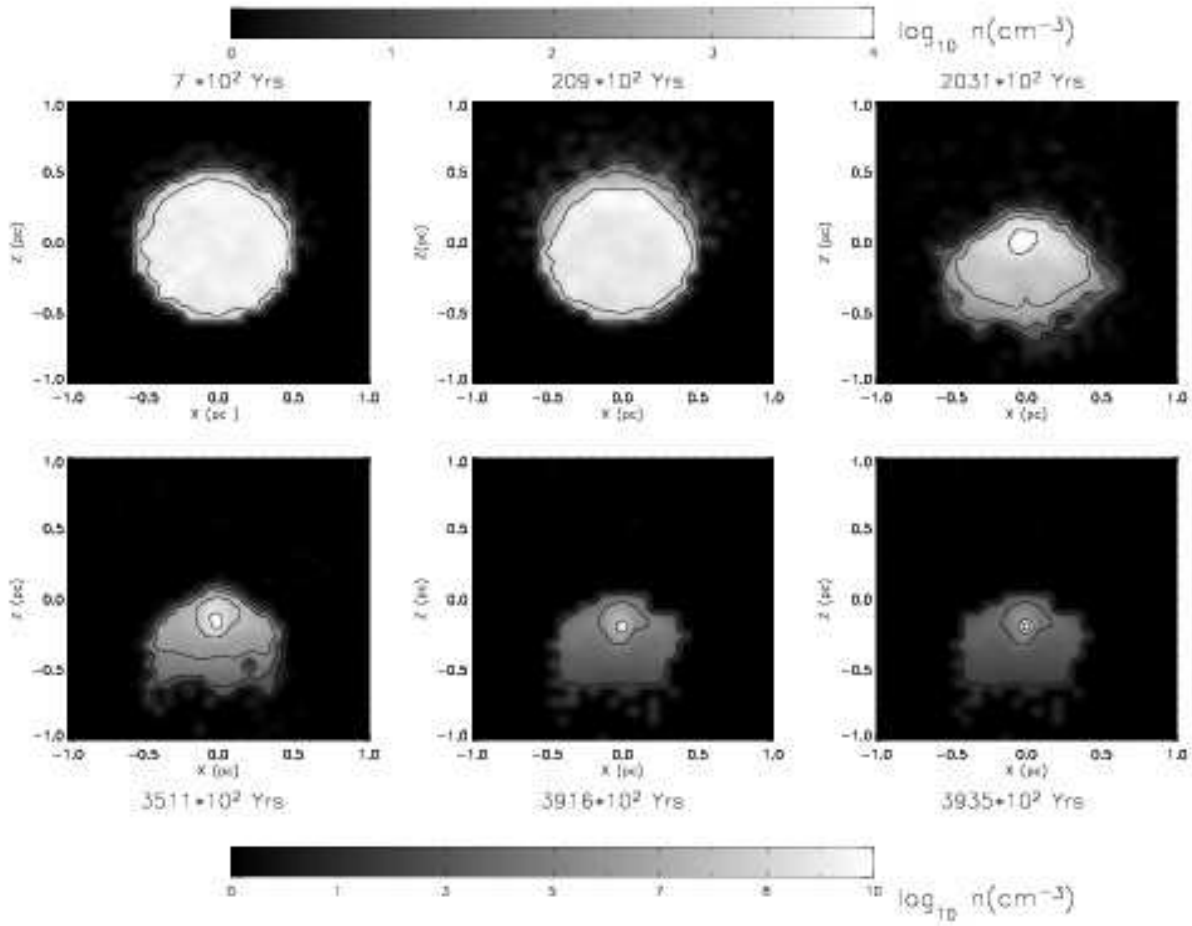

Fig. 2.— The evolutionary snapshots of the number density of the simulated molecular cloud A at the cross section $y = 0$ from $t = 700$ years to $t = 0.394$ My. The top grey bar shows the density scale in logarithm for the upper row snapshots and the bottom bar for the second row snapshots.

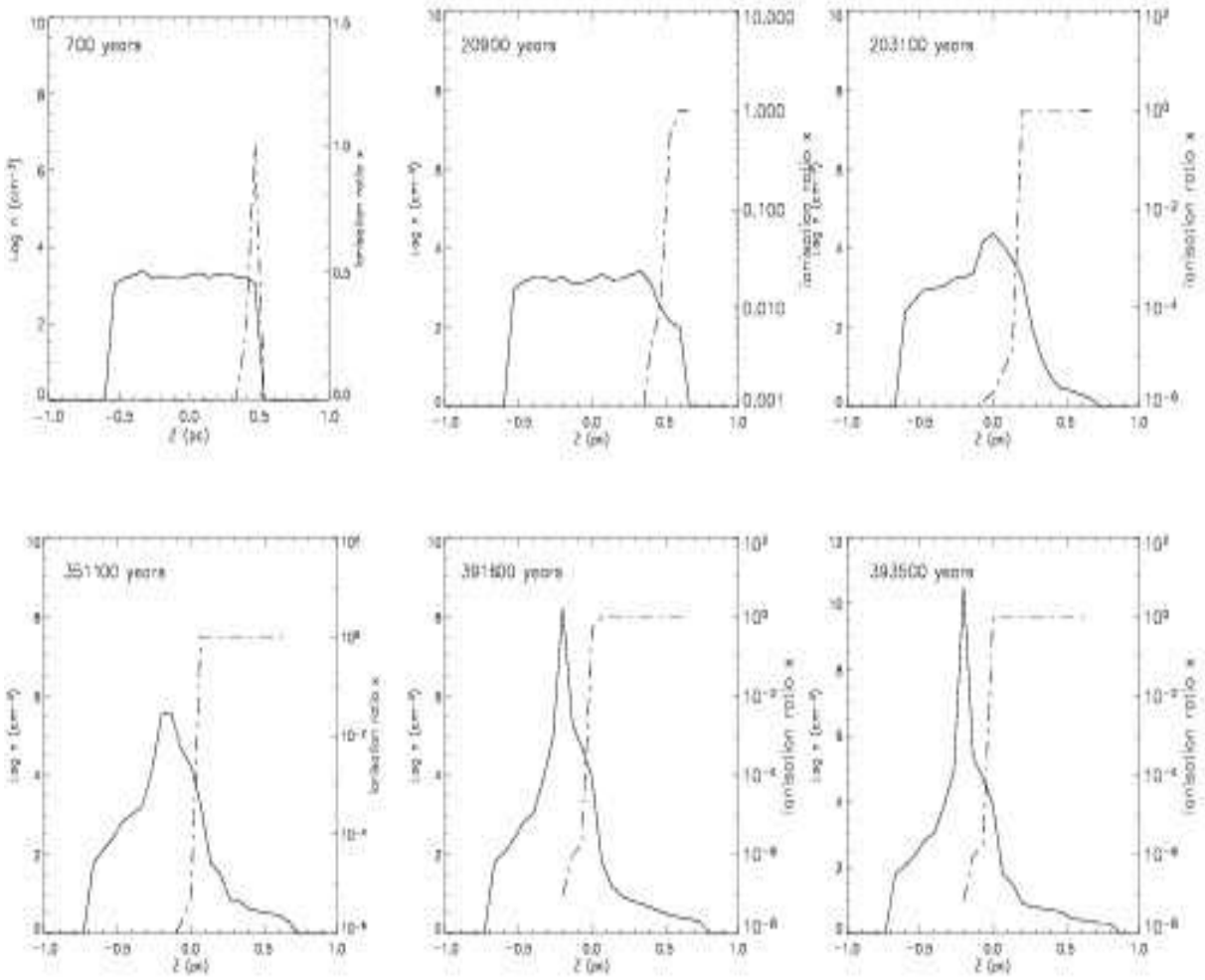

Fig. 3.— The distributions of the number density (solid line) and ionisation ratio x (dot-dashe line) of the simulated molecular cloud A along the symmetrical axis z from $t = 700$ years to $t = 0.394$ My.

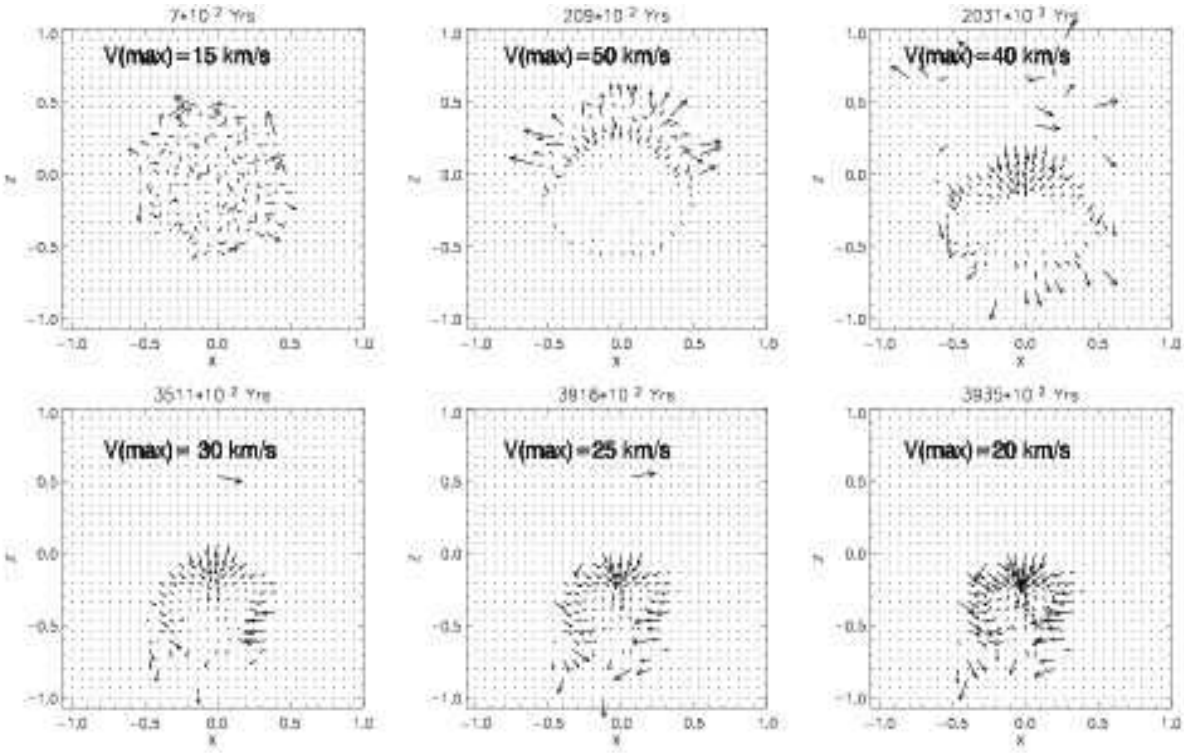

Fig. 4.— The evolution of the velocity field for the same cloud as in Figure 2 over a period of 0.394 My. The length of the arrow indicates the magnitude of velocity and the maximum magnitude of the velocities at different stages of the evolution have been written inside the corresponding panels.

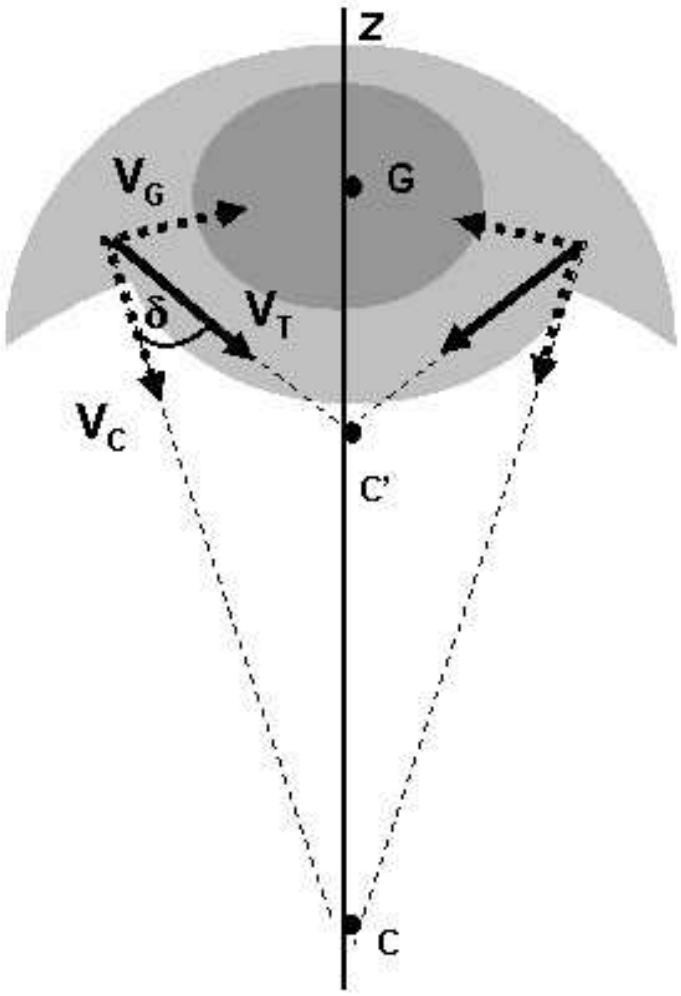

Fig. 5.— An illustration about the effect of the gravity of the main body of the cloud on the velocity of the shocked gas particle in the 'ear-like' structures at the two sides of the cloud. The central solid lines are their structure symmetrical line z.

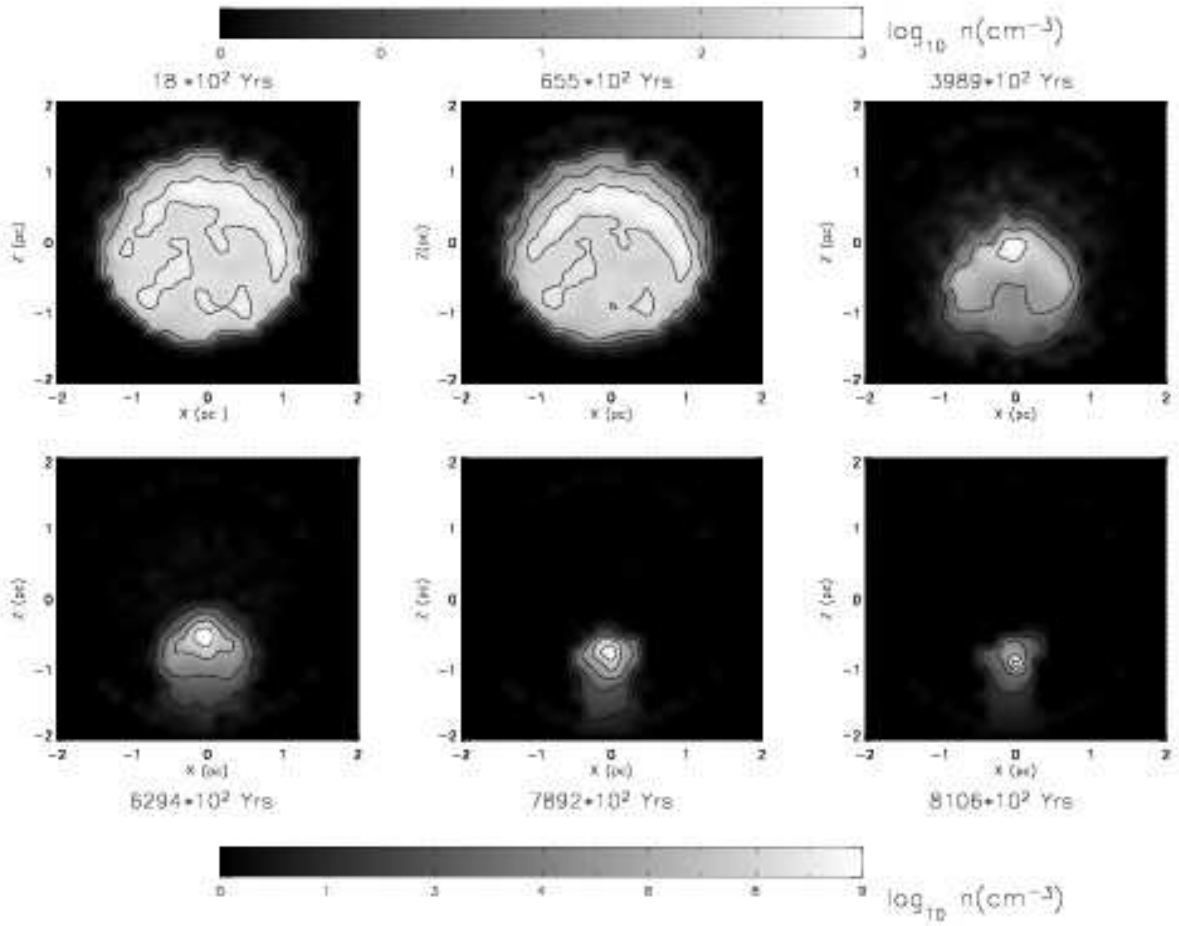

Fig. 6.— The evolutionary snapshots of the number density of the simulated molecular cloud B at the cross section $y = 0$ from $t = 1800$ years to $t = 0.81$ My. The top grey bar shows the density scale in logarithm for the upper row snapshots and the bottom bar for the second row snapshots.

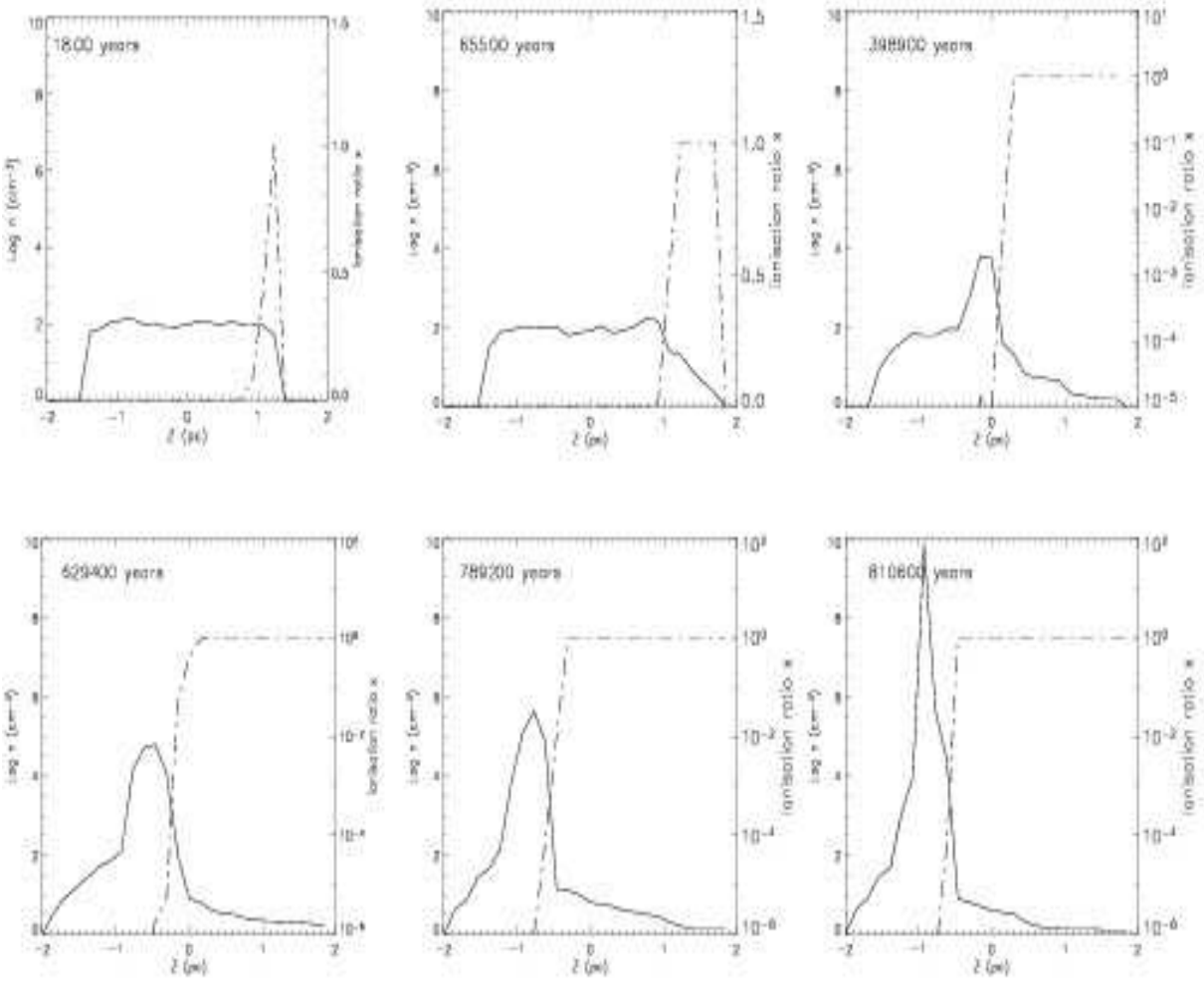

Fig. 7.— The distributions of the number density (solid line) and ionisation ratio x (dot-dashe line) of the simulated molecular cloud B along the symmetrical axis z from $t = 1800$ years to $t = 0.81$ My.

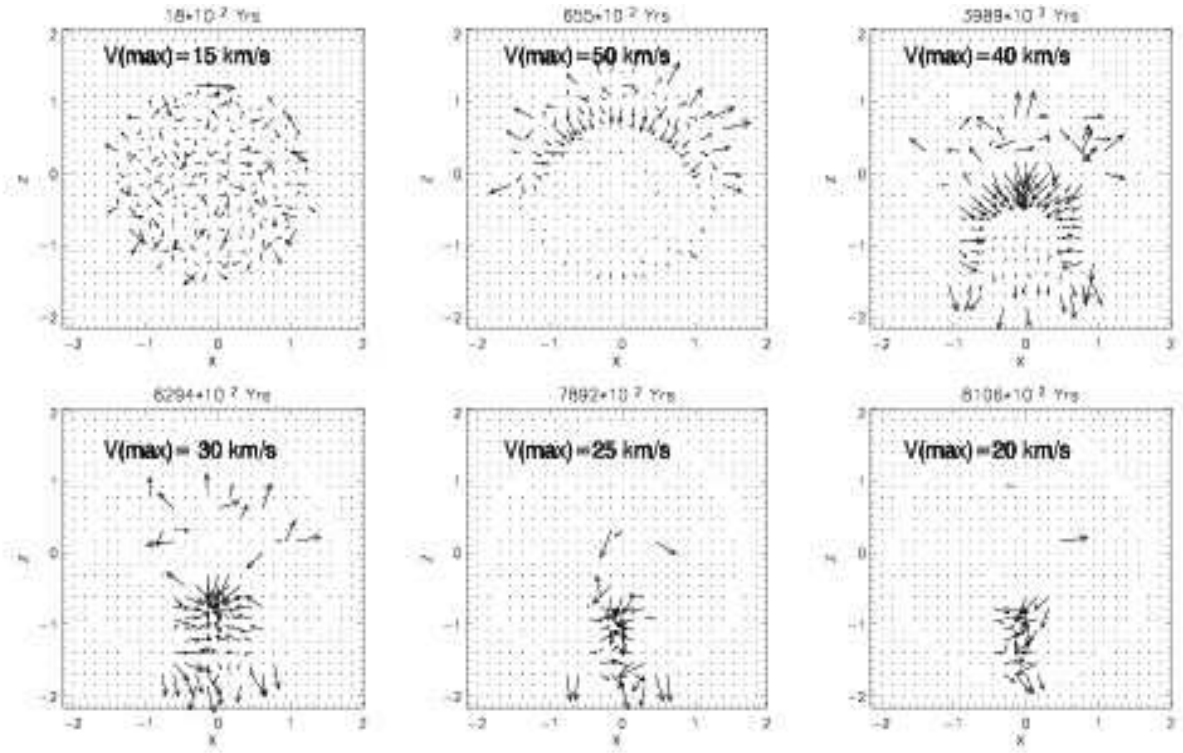

Fig. 8.— The evolution of the velocity field for the same cloud as in Figure 6 over a period of time of 0.81 My. The length of the arrow indicates the magnitude of velocity and the maximum magnitude of the velocities at different stages of the evolution have been written inside the corresponding panels.

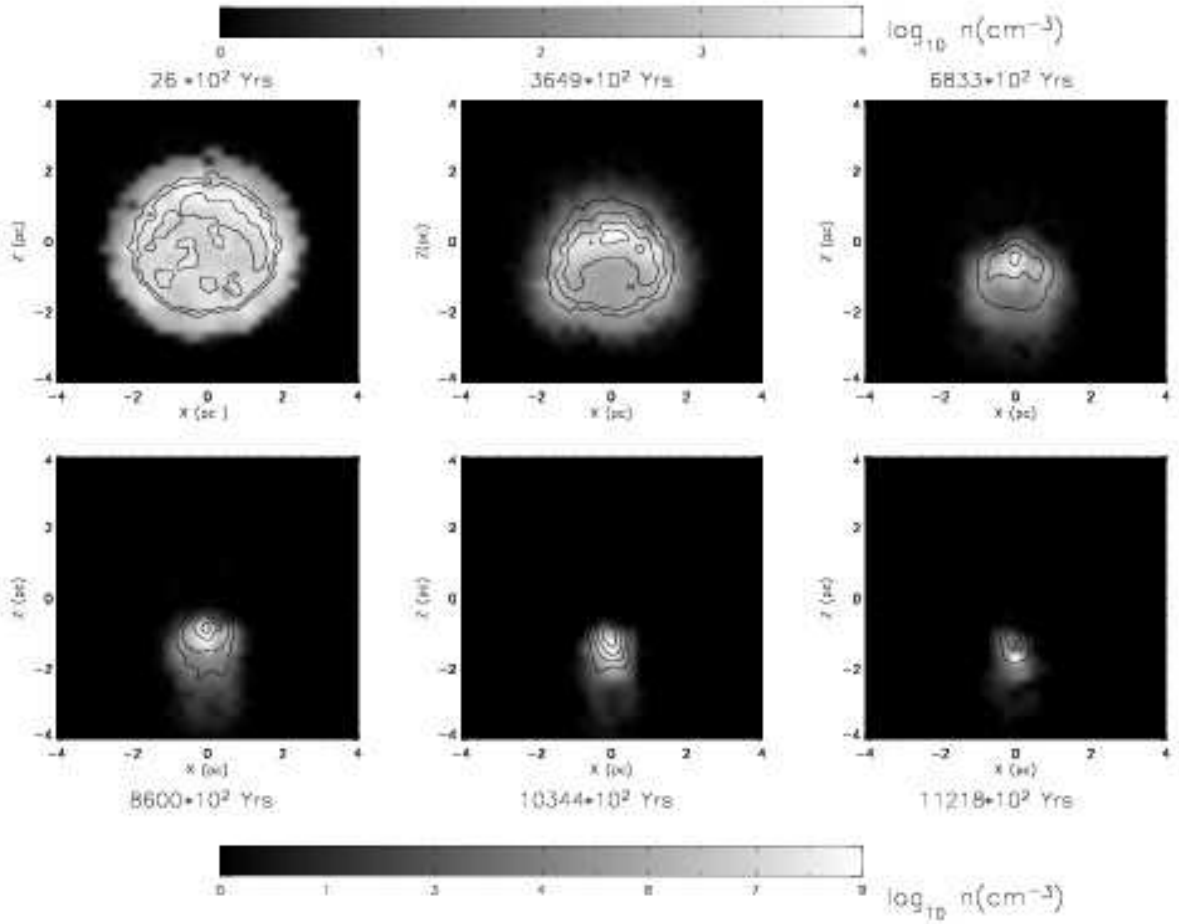

Fig. 9.— The evolutionary snapshots of the number density of the simulated molecular cloud C at the cross section $y = 0$ over a period of 1.12 My. The top grey bar shows the density scale in logarithm for the upper row snapshots and the bottom bar for the snapshots in the bottom row.

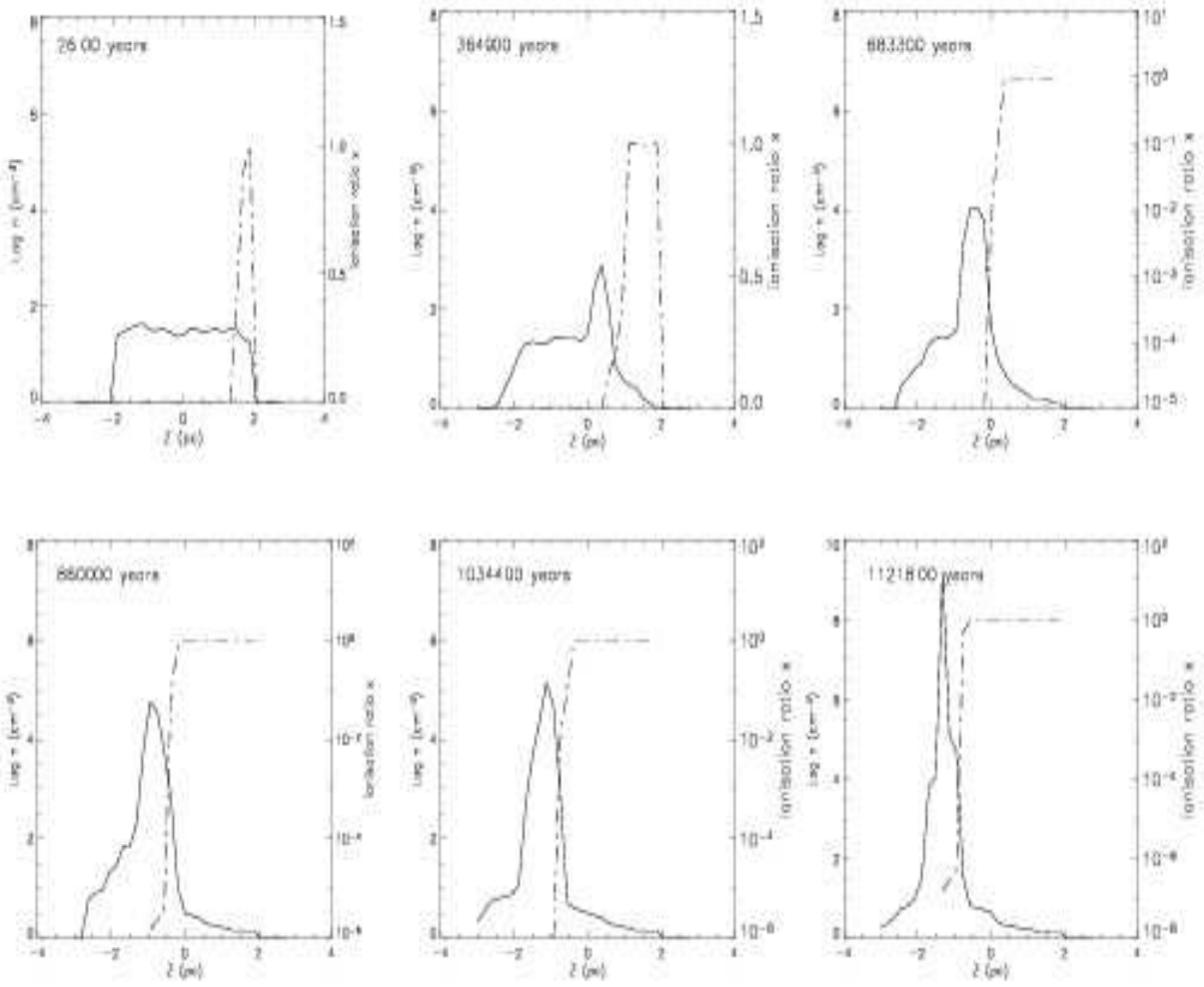

Fig. 10.— The distributions of the number density (solid line) and ionisation ratio x (dot-dashe line) of the simulated molecular cloud C along the symmetrical axis $x = 0$ over a period of 1.12 My.

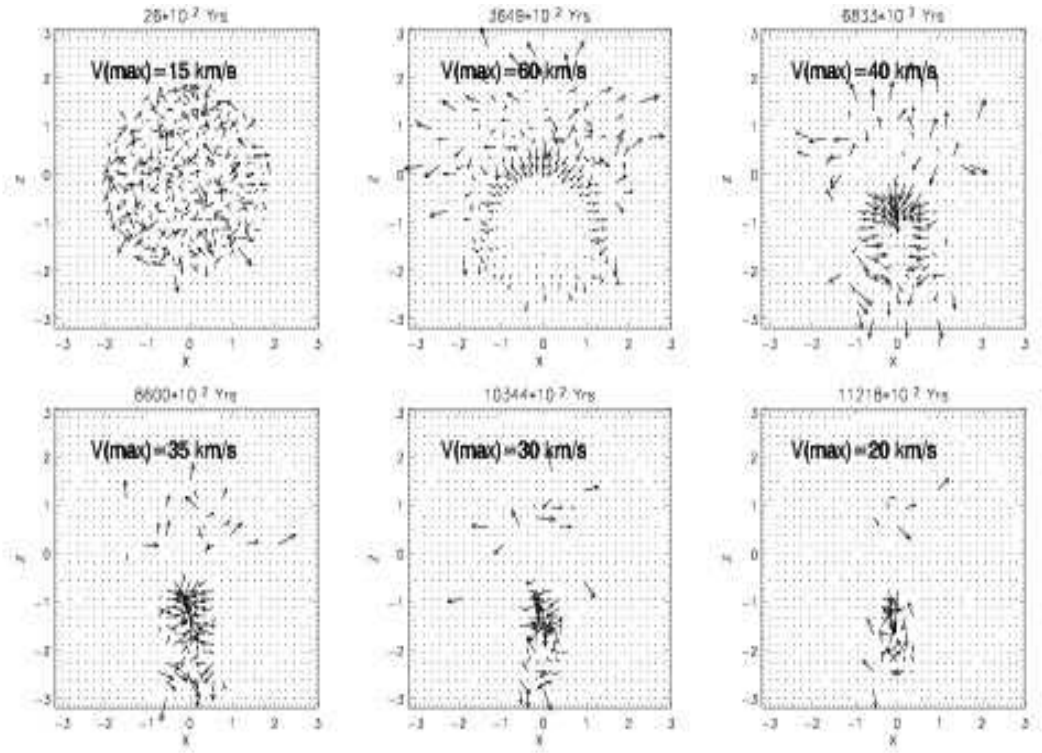

Fig. 11.— The evolution of the velocity field for the same cloud as in Figure 9 over the same period of time. The length of the arrows indicates the magnitude of velocity and the longest arrow in each panel represents the maximum velocity in the corresponding velocity field distribution at different stages of the evolution.

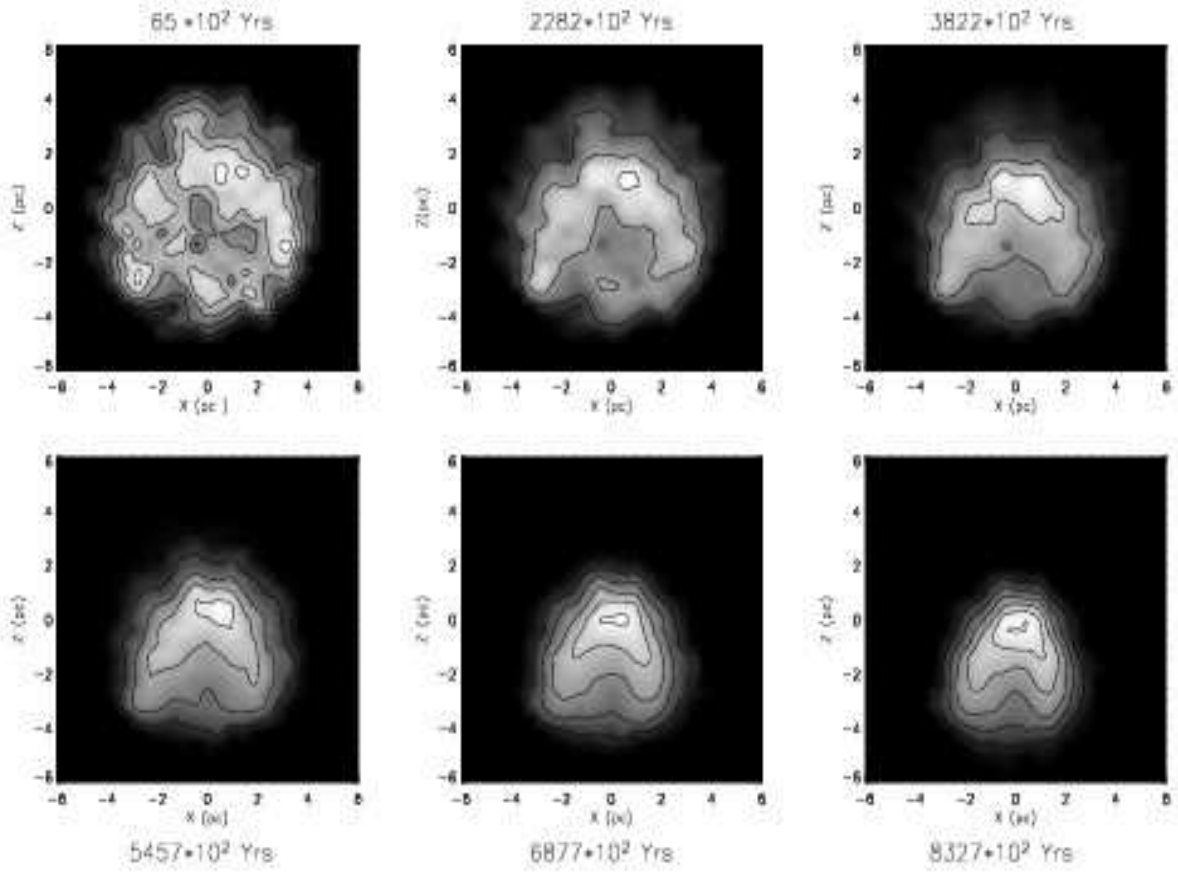

Fig. 12.— The growth and smooth processes of the large-scale surface instability over the evolutionary process in cloud D.

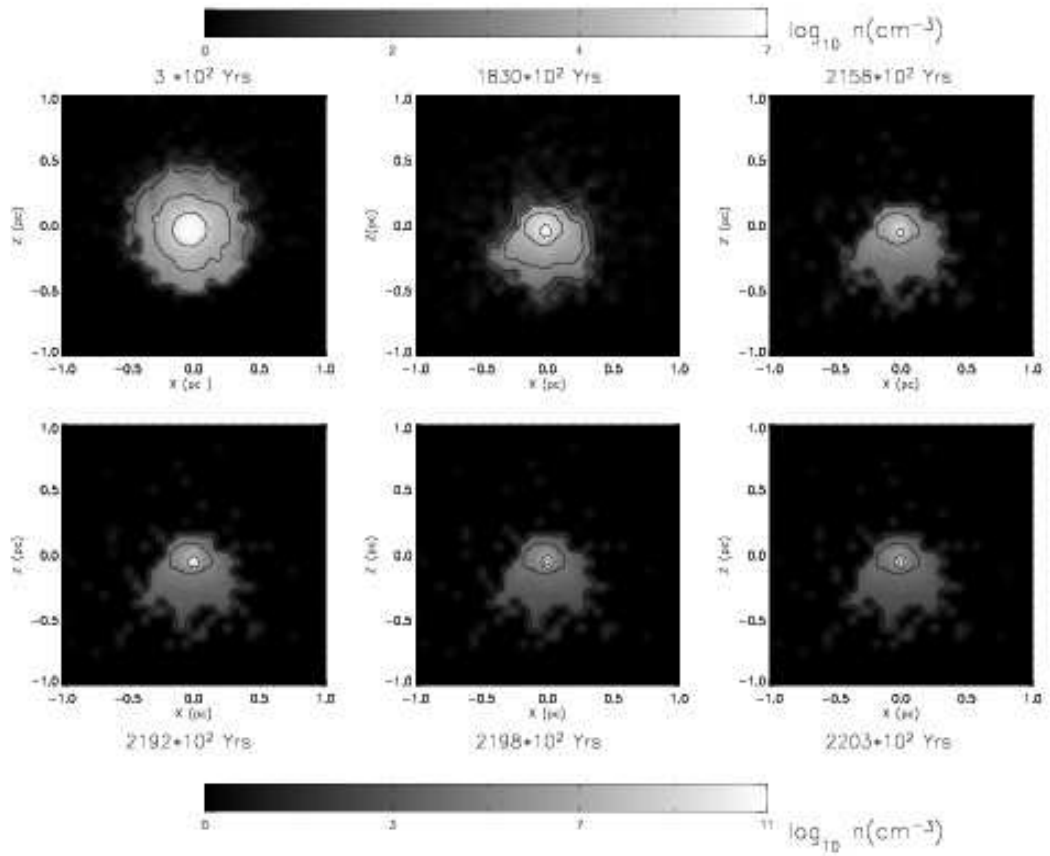

Fig. 13.— The evolutionary snapshots of the number density of the simulated molecular cloud A with an initial core-halo distribution at the cross section $y = 0$. The top grey bar shows the density scale in logarithm for the upper row snapshots and the bottom bar for the second row snapshots.

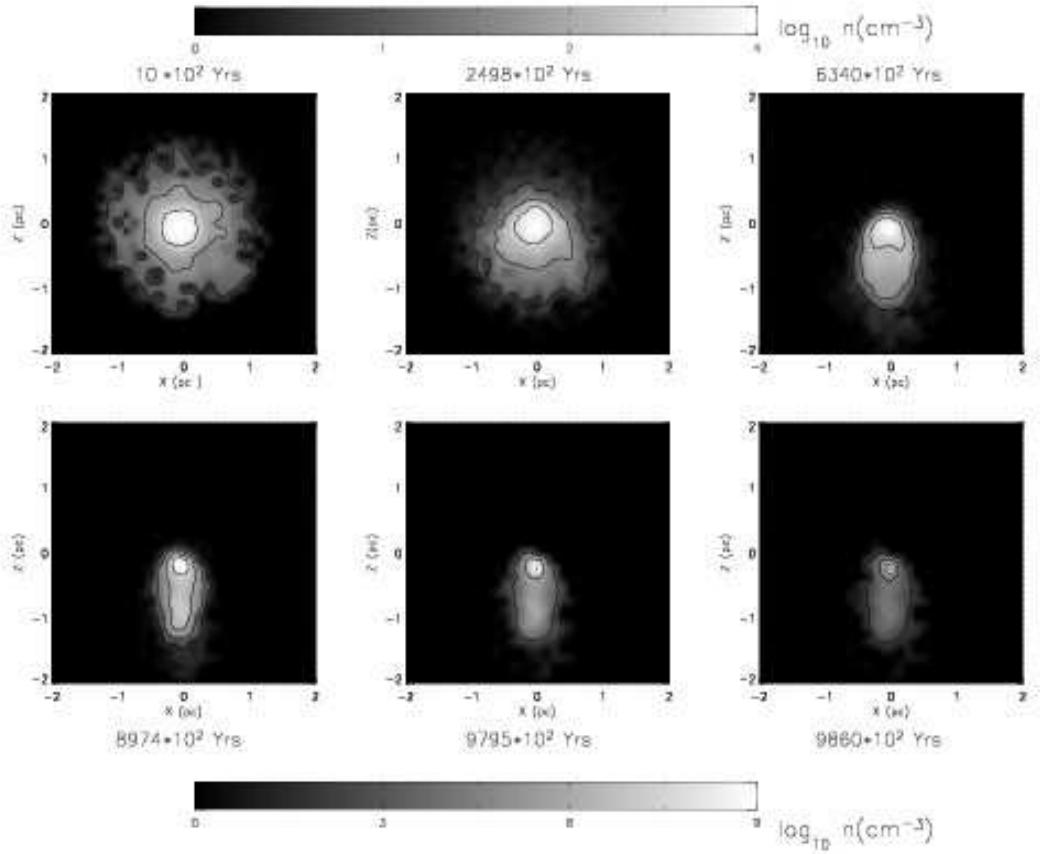

Fig. 14.— The evolutionary snapshots of the number density of the simulated molecular cloud B with an initial core-halo distributionat the cross section $y = 0$. The top grey bar shows the density scale in logarithm for the upper row snapshots and the bottom bar for the second row snapshots.

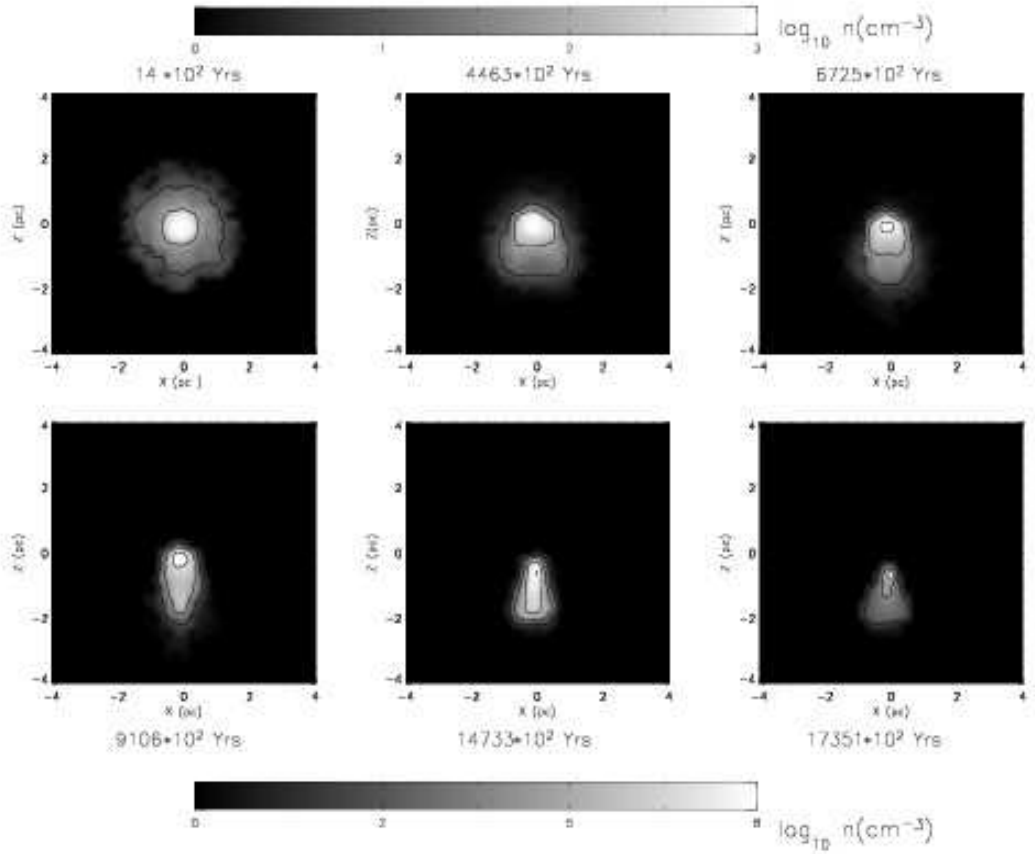

Fig. 15.— The evolutionary snapshots of the number density of the simulated molecular cloud C with an initial core-halo distributionat the cross section $y = 0$. The top grey bar shows the density scale in logarithm for the upper row snapshots and the bottom bar for the second row snapshots.

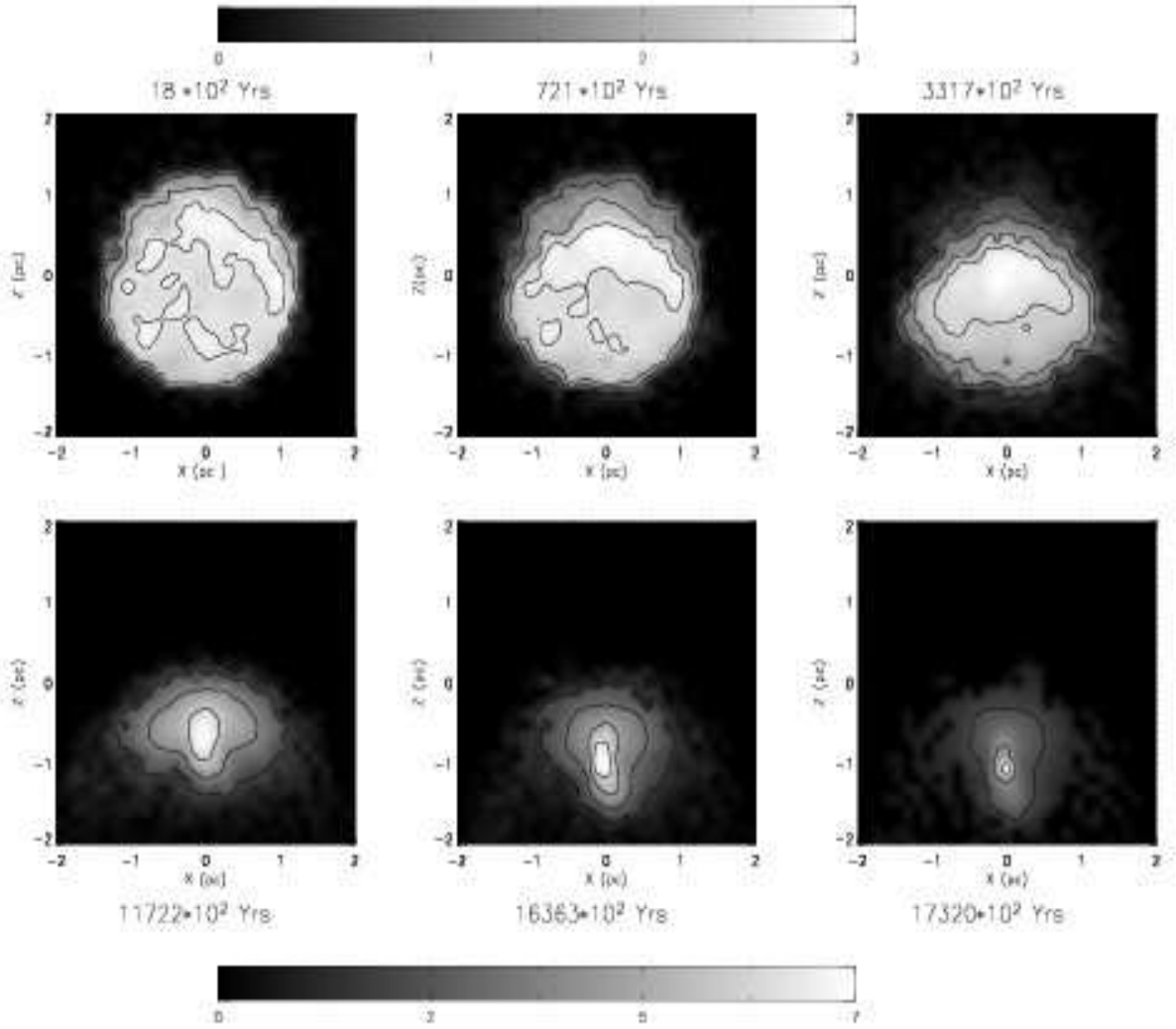

Fig. 16.— The evolutionary snapshots of the number density of the simulated molecular cloud B with a zero external pressure boundary at the cross section $y = 0$. The top grey bar shows the density scale in logarithm for the upper row snapshots and the bottom bar for the snapshots in the bottom row.

[1]Morphology type

[2]Core formation time in My

[3]Core collapse time in My

Table 1. Parameters of set one clouds

Cloud	Δ	Γ	$n_0(cm^{-3})$	R(pc)	Region	M type[1]	CFT[2]	CCT[3]
A	0.68	55	2672	0.5	V	A	0.35	0.39
B	7.3	89.1	152	1.3	III	B	0.63	0.6
C	18	108	49	1.9	III	C	0.86	1.12
D	182	169	3.2	4.7	III	C	1.0	N/A

[123]They have the same meanings as that in Table 1.

Table 2. Parameters of second set clouds

Cloud	Δ	Γ	$n_0(cm^{-3})$	M($M_\odot$)	Region	M type[1]	CFT[2]	CCT[3]
A	0.68	55	2672	35	V	A	0.35	0.39
A'	1.94	55	916	12	V	B	0.45	0.55
A"	2.9	55	610	8	III	C	0.48	0.72
A"'	23	55	76	1	III	C	0.25	N/A